RNA (1997), 3:157–174. Cambridge University Press. Printed in the USA.

Antisense RNA control of gene expression in bacteriophage P22. II. Kinetic mechanism and cation specificity of the pairing reaction

KATHERINE L. SCHAEFER[1] and WILLIAM R. McCLURE
Department of Biological Sciences, Carnegie Mellon University, Pittsburgh, Pennsylvania 15213, USA

ABSTRACT

The bacteriophage P22 sar RNA–ant mRNA pairing reaction was characterized kinetically. The pairing reaction proceeds by a three-step pathway. First, reversible base pairs form between complementary hairpin loops in sar RNA and ant RNA (K_d = 270 nM). Next, stable duplex formation initiates between single-stranded nucleotides in sar RNA and ant RNA; the ant RNA nucleotides are at the bottom of a hairpin stem that is partially accessible. Concomitant unwinding of one sar RNA hairpin and the complementary ant RNA hairpin then occurs, to form a partially paired intermediate (k_2 = 12 min^{-1}). Finally, a complete duplex forms after unwinding of the other sar RNA hairpin and the complementary ant RNA hairpin (k_3 = 7 min^{-1}). Experiments with sar RNA sequence and length variants demonstrate that the precise structures of both sar RNA hairpins affect the kinetic parameters. The pairing reaction is Mg^{2+}-dependent, and shows high specificity for the required cation. Maximal pairing rates are achieved when more than one Mg^{2+} ion is bound. The cation-dependence and specificity indicate a requirement for Mg^{2+}-dependent tertiary structure.

Keywords: Mg^{2+}; pairing pathway; reversible base pairs; RNA structure

INTRODUCTION

The overall kinetics of duplex formation between highly structured antisense RNAs and target RNAs are similar to those observed with unstructured oligomers. Second-order rate constants for duplex formation between two oligomers at 37 °C range from 0.3 to 8×10^6 M^{-1} s^{-1} in monovalent salt buffers (Cantor & Schimmel, 1980). The pairing of an antisense RNA to a target RNA is a more complicated process than the pairing of two small, unstructured RNAs, because many of the nucleotides in antisense RNAs and target RNAs are found in hairpin stems or other intramolecular structures. These intramolecular interactions must be disrupted before a complete duplex can be formed. Because the unwinding of hairpin stems is a slow process compared to intermolecular helix propagation (Cantor & Schimmel, 1980), pairing pauses can occur when hairpins (or other structures) must be disrupted. If a stable complex has not been formed before a pairing pause occurs, the initial complex can dissociate. Despite this complication, second-order rate constants for formation of the first stable duplex in antisense RNA–target RNA pairing reactions are between 0.1 and 3×10^6 M^{-1} s^{-1}, indicating that formation of at least a partially paired complex can proceed at rates similar to those observed with unstructured oligonucleotides (Tomizawa, 1984; Persson et al., 1988; Kittle et al., 1989; Sugiyama & Itoh, 1993; van Biesen et al., 1993; Siemering et al., 1994; Thisted et al., 1994).

Specific antisense RNA–target RNA pairing mechanisms allow the limitations imposed by intramolecular RNA secondary structure to be overcome; conversely, disruptions in features of the RNAs necessary for pairing reduce rate constants by at least 2–3 orders of magnitude (Persson et al., 1990; Tomizawa, 1990b; Sugiyama & Itoh, 1993; Siemering et al., 1994; Thisted et al., 1994). Three classes of pairing pathways that result in rapid formation of a stable complex have been observed. In the first type, seen in the sok RNA-mok/hok RNA pairing reaction from the plasmid R1 (Thisted et al., 1994), a stable complex forms between nucleotides in long, complementary, single-stranded regions. A second (and similar) mechanism is observed in the RNA•OUT–RNA•IN pairing reaction from the insertion sequence IS10 (Kittle et al., 1989): a stable complex forms between a long, single-stranded region and a large hair-

Reprint requests to: William R. McClure, Department of Biological Sciences, Carnegie Mellon University, Pittsburgh, Pennsylvania 15213, USA; e-mail: wm0p@andrew.cmu.edu.
[1]Present address: Department of Molecular and Cellular Biology, Harvard University, Cambridge, Massachusetts 02138, USA.

pin loop. In many cases, long, complementary single-stranded regions are not present. In these cases, a third type of mechanism (the "loop-loop" mechanism) is used. Pairing begins with the formation of several reversible base pairs between nucleotides in loops, followed by stable duplex formation initiating between nucleotides in short, single-stranded regions. The increased stability conferred by the loop-loop interactions allows the RNAs to remain paired while some intramolecular structure is disrupted and a stable duplex forms. The RNA I-RNA II pairing reactions of the Col E1 plasmid (Tomizawa, 1984) and the plasmid pMU 720 (Siemering et al., 1994), the cop A RNA-cop T RNA pairing reaction from the plasmid R1 (Persson et al., 1990), the RNA I-rep RNA pairing reaction from the Col E2 plasmid (Sugiyama & Itoh, 1993), and the finP RNA-traJ RNA pairing reaction from the IncF1 incompatibility group plasmids (van Biesen et al., 1993) all use variations on this mechanism.

The rate of pairing of an antisense RNA to a target RNA is affected by the structures of both RNAs in at least two ways. First, the structures of the antisense RNA and the target RNA affect the pairing rate by dictating the choice of mechanism used. The highest pairing rate constants are achieved using the loop-loop mechanism; the average second-order rate constant for formation of the first stable duplex in a pairing reaction using a loop-loop mechanism is 10-fold higher than the rate constants for the other two types of mechanisms. Second, the precise nature of the structures in both RNAs can affect the pairing rate by affecting the rate of hairpin disruption (Hjalt & Wagner, 1995) and (in loop-loop type mechanisms) the strength of the initial reversible base pairs (Grosjean et al., 1976; Eguchi & Tomizawa, 1991; Gregorian & Crothers, 1995).

We have further characterized the sar RNA-ant RNA pairing reaction from the bacteriophage P22 (Liao et al., 1987; Wu et al., 1987). Pairing proceeds by a three-step, loop-loop type pathway. The effect of structure on the pairing reaction was investigated in two ways. First, the effects of sar RNA mutations on the pairing pathway were examined and compared to the effects on sar RNA structure (Schaefer & McClure, 1996). Second, because Mg^{2+} affects RNA structure, the Mg^{2+}-dependence of the pairing reaction was compared to the Mg^{2+}-dependence of sar and ant RNA structure formation (Schaefer & McClure, 1996). The results of this analysis suggest that the precise structure of sar RNA, and possibly of ant RNA, affects both the rate of hairpin disruption and the strength of the initial complex.

RESULTS

The first pairing step is reversible

In order to determine if the first step in the sar RNA-ant RNA pairing reaction is reversible, we measured pseudo-first-order (ant RNA in excess) rate constants (k_{obs}) over a range of ant RNA concentrations, using an electrophoretic mobility shift (gel-shift) assay. The relationship between k_{obs} and A_0 reveals whether initial, reversible steps occur. For a reaction with no reversible steps:

$$A + S \xrightarrow{k} \text{stably paired complex(es)}, \quad (1)$$

$k_{obs} = k \cdot A_0$. Alternatively, for a reaction with reversible step(s) followed by irreversible step(s):

$$A + S \overset{K_d}{\rightleftharpoons} C \xrightarrow{k_2} \text{stably paired complex(es)}, \quad (2)$$

$k_{obs} = k_2 \cdot A_0 / K_d + A_0$.

The experiments of Figure 1 examine the dependence of k_{obs} on A_0. The pairing rate was constant over > 75% of the reaction (Fig. 1B), indicating that the majority of the sar RNA used was functionally homogenous. The slope of 0.69 min^{-1} at 15 nM ant RNA corresponds to a second-order rate constant of 7.7×10^5 M^{-1} s^{-1}. A plot of k_{obs} versus ant RNA concentration (Fig. 1C) was hyperbolic, indicating that the sar RNA-ant RNA pairing reaction begins with at least one reversible step. Values of K_d (the concentration at the half-maximal k_{obs}) and k_2 (the maximum k_{obs}) were determined as described in Materials and Methods (Fig. 1D). K_d was 270 nM and k_2 was 12 min^{-1}.

Pairing proceeds through a stable intermediate

The band corresponding to the sar RNA-ant RNA complex in the gel-shift assays could in fact be a mixture of stably paired intermediate(s) and fully paired duplex. The presence of stable reaction intermediates was investigated using an RNase protection assay. Because the high concentration of RNase A used in these assays digests all single-stranded (unpaired) regions of the RNA, appearance of only a full-length protected fragment would indicate that pairing intermediates are undetectable. Conversely, the appearance and subsequent disappearance of shorter fragments would provide evidence that the pairing reaction proceeds through stable intermediate(s) before complete duplex formation. The experiments of Figure 2A and B indicate that the pairing reaction proceeds through a stable intermediate. Protected fragments smaller than full-length sar RNA appeared, and then disappeared, as the pairing reaction proceeded. These protected fragments were observed both in reactions with 5′ end-labeled sar RNA and in reactions with 3′ end-labeled sar RNA.

The RNase A used in the RNase protection assays cleaves the labeled sar RNA at all highly accessible sites (for sar RNA, these are nt 2, 3, 13, 14, 22, 28, 31, 32, and 47; Schaefer & McClure, 1996). In addition,

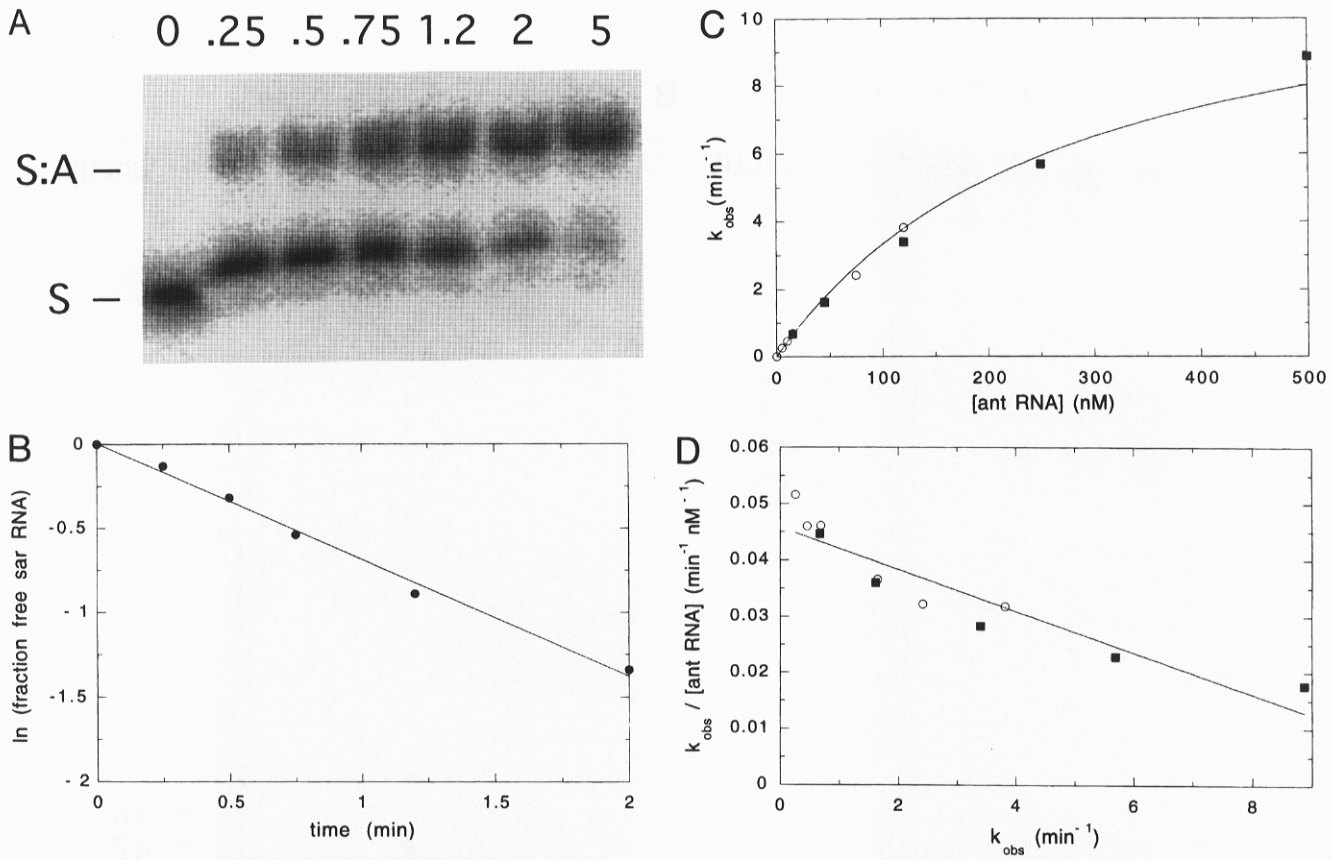

FIGURE 1. Kinetics of the sar RNA–ant RNA pairing reaction. Pairing reactions were performed at 37 °C in the presence of 10 mM Mg^{2+} with 5′ end-labeled sar RNA (≤1.5 nM) and the indicated ant RNA concentrations. At the times indicated, portions of the reaction were quenched by addition of EDTA. The sar RNA–ant RNA complexes (S:A) were separated from free sar RNA (S) on a 5% polyacrylamide gel. **A:** An AMBIS scan from a gel-shift experiment with 15 nM ant RNA is shown. Times (min) are indicated above the lanes. **B:** Rate constant determination from the experiment in A. The fraction of free sar RNA is plotted logarithmically versus time. The *y* axis value at 5 min was −2.25. k_{obs} (0.69 min^{-1}) was determined from the slope. **C:** The dependence of k_{obs} on ant RNA concentration. k_{obs} is plotted versus ant RNA concentration. Results of two experiments are shown, using different symbols. The line corresponds to the values of K_d and k_2 in D. **D:** Determination of K_d and k_2 from the data of C using Equation 3 in the Materials and methods. k_{obs} / ant RNA concentration is plotted versus k_{obs}. The line is a linear least-squares fit; K_d = 270 ± 30 nM; k_2 = 12 ± 1 min^{-1}.

because the concentration of RNase A is very high, sar RNA is sometimes cleaved at less accessible nucleotides that are involved in intramolecular nucleotide interactions. The size of the protected fragments allows inferences to be made about those portions of the molecule that are involved in stable intermolecular base pairs at the time of RNase addition.

The absence of sar RNA fragments longer than 4 nt in the 0-min samples (data not shown) shows that the concentrations of RNase used in these experiments were sufficient to cleave unpaired sar RNA at nt 2 and 3 (5′ end-labeled fragments) or at nt 64 and/or 67 (3′ end-labeled fragments). Therefore, the appearance during the pairing reaction of 5′-labeled fragments larger than 3 nt and 3′-labeled fragments larger than 4 nt indicates that the 5′ and 3′ ends are both paired in the intermediate.

The length of the protected fragments (Fig. 2C) shows that sar RNA nt 1–32 and 65–68 are paired to ant RNA in the intermediate. 5′ End-labeled fragments resulting from cleavages at nt 13, 14, 31, or 32 were not seen, indicating that at least the first 32 nt of sar RNA are paired in the intermediate. Similarly, the appearance of 3′ end-labeled fragments longer than 4 nt indicates that nt 65–68 are paired to ant RNA in the intermediate.

The family of 5′ end-labeled fragments caused by cleavages at sar RNA nt 39, 40, 43, and 44, and the group of 3′-labeled fragments resulting from cleavages at sar RNA nt 46, 47, 49, 50, 52, and 56, indicate that sar RNA hairpin II is not fully paired to ant RNA in the intermediate. Sar RNA is probably paired to ant RNA only through nt 32 in the intermediate. In this model, the family of cleavages in sar RNA stem II result from accessibility of the hairpin stem to the large quantities of RNase used in the experiment; the lack of cleavage at nt 37 and 38 simply reflects the differential susceptibility of various paired stem nucleotides to the (single-strand-specific or ss-specific) RNase. This model is further supported by the observation that a fragment of length 47 (resulting from cleavage in the single-

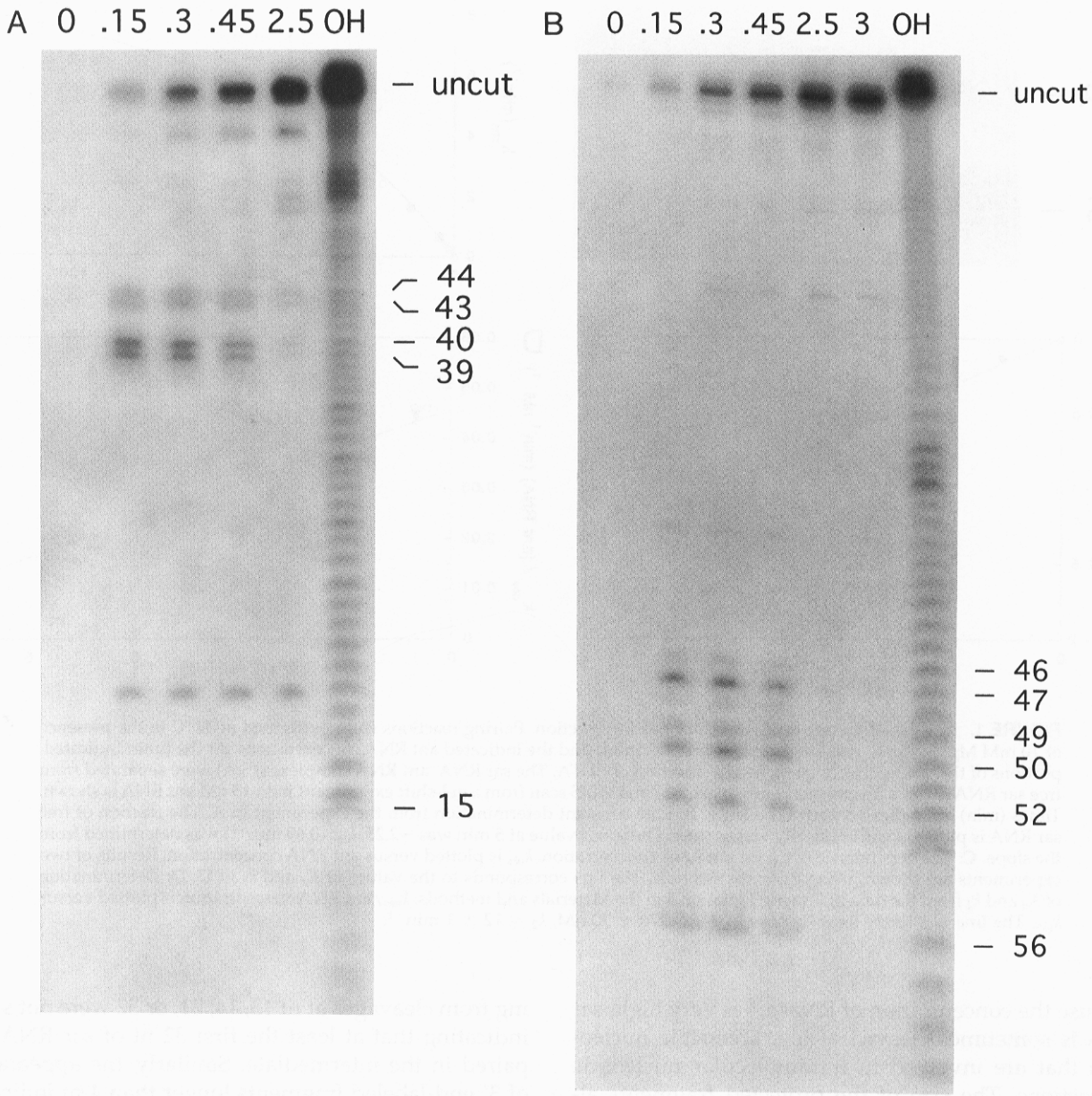

FIGURE 2. Kinetic characterization of the pairing reaction intermediate. Pairing reactions were performed at 37 °C with sar RNA concentrations ≤ 1.5 nM; ant RNA concentrations are indicated below. At times (min) indicated above the lanes, the pairing reaction was terminated by the addition of RNase A to digest unpaired RNAs. The protected RNA fragments were separated on a 10% polyacrylamide sequencing gel. Fragment sizes were determined by comparison with an alkaline hydrolysis marker ladder (OH). The number next to each band indicates the sar RNA nucleotide after which RNase cleaved. **A:** Autoradiograph from a RNase protection experiment with 5′ end-labeled sar RNA and 101 nM ant RNA. **B:** Autoradiograph from a RNase protection experiment with 3′ end-labeled sar RNA and 65 nM ant RNA. **C:** Schematic representation of sar RNA. Open arrows are cleavage sites observed with 5′ end-labeled RNA; filled arrows are cleavage sites observed with 3′ end-labeled RNA. **D,E:** Determination of k_3 from the experiments of A and B, respectively. Lines correspond to the values for k_3 (determined using Equations 4 and 5 in Materials and Methods) and the values of K_d and k_2 (determined from the experiment of Fig. 1). Because it was impossible to take more than three time points during that fraction of the reaction where the intermediate was present in significant amounts, values of k_3 (Table 1) were determined by performing experiments like those in A and B multiple times and taking the average of the k_3 values obtained in each experiment. The fraction of RNA in the intermediate complex (●, solid line) or fully paired complex (□, dashed line) is plotted versus time. At t = 2.5 min (D) or 3 min (E), the fraction of RNA in the intermediate complex had reached 0 and the fraction of RNA in the fully paired complex had reached 1.0. The RNA fragments slightly smaller than full length (A) were treated as fully paired. The 20-mer (A) and the minor RNA fragments larger than the intermediate (A, B) were neglected in the analysis because they did not appear reproducibly in all experiments. (*Figure continues on facing page.*)

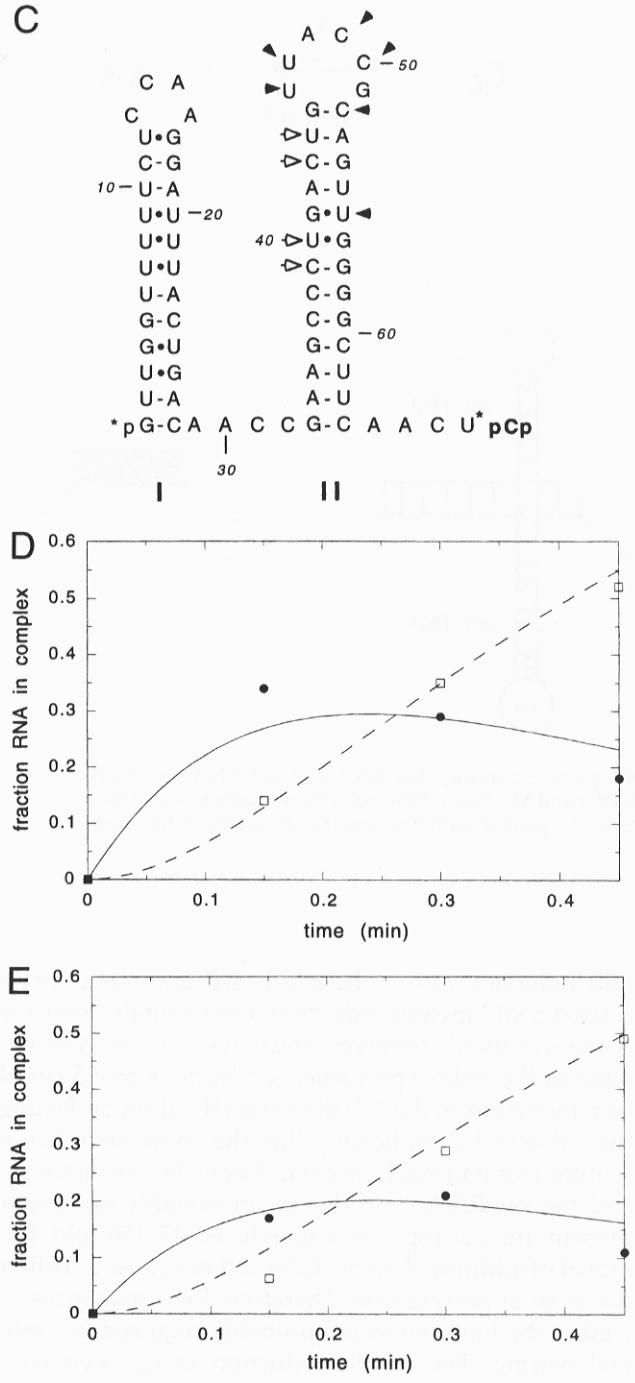

FIGURE 2. (*Continued.*)

stranded loop) that exhibits the same kinetics as the group of fragments observed in the experiments of Figure 2 was detected in RNase protection assays done with reduced quantities of RNase (data not shown). However, it is formally possible that the bottom of sar RNA stem II up to nt 38 is paired to ant RNA in the intermediate and that the extent of sar RNA hairpin II unwinding and pairing to ant RNA is heterogeneous.

The value of k_3 (the rate constant corresponding to conversion of the stable intermediate to the fully paired complex) was determined from the experiments of Figure 2A and B, as described in Materials and Methods (Fig. 2D,E). k_3 was 7 min^{-1} (Table 1). The fact that one value of k_3 can explain both the rate of appearance of fully paired complex and the rate of appearance and subsequent disappearance of the intermediate indicates that essentially all of the pairing is proceeding through the intermediate, and not through another pathway containing another intermediate.

A summary of the results described above is shown in Figure 3. The transient intermediate (C_t) was inferred because a reversible step was detected, requiring a dissociable intermediate. The intermediate observed in the RNase protection experiments (C_c, or the committed complex) cannot be the transient intermediate because the C_c intermediate was resistant to large quantities of RNase for $\geq$ 10 min; thus, the base pairs formed are not unpaired to any detectable extent.

Changes in both halves of sar RNA affect the pairing reaction

To explore how the structure of sar RNA affects the pairing reaction, we measured pairing rate constants for sar RNA variants, using the experimental techniques and analysis described above.

The experiments of Figure 4A indicate that removal of the 3′ half of sar RNA drastically impairs its ability to pair to ant RNA. "Sar-34 RNA" is missing nt 35–68 and thus does not have hairpin II or the 3′ tail. In the limit of low ant RNA concentration, the k_{obs} for the sar-34 RNA–ant RNA reaction was approximately 15-fold lower than that for the reaction containing wild-type sar RNA, showing that the 3′ half of the molecule is crucial for pairing. A plot of k_{obs} versus A_0 was linear over the entire concentration range tested (up to 400 nM), indicating that $K_d \gg 400$ nM (Fig. 4; Table 1).

In addition, the experiments of Figure 4A indicate that two different sar RNA loop I mutations affect both K_d and k_2 (Fig. 4; Table 1) but not k_3. The 12U → A

TABLE 1. Summary of the kinetic parameters obtained for pairing reactions with various sar RNAs.[a]

sar RNA	K_d (nM)	k_2 (min^{-1})	k_3 (min^{-1})	k_2/K_d (M^{-1} s^{-1})
Wild type	270 (30)	12 (1)	7 (2)	7.6×10^5
12U → A	190 (30)	8 (1)	5 (2)	7.0×10^5
13C → U	110 (20)	2.0 (0.3)	7 (2)	2.9×10^5
sar-34	≫400	nd	na	3.9×10^4

[a]Values were determined from the experiments of Figures 1, 2, and 4; standard deviations are given in parentheses. k_3 values are the result of six (wild-type sar RNA) or two (12U → A and 13C → U RNAs) determinations. nd, not determined. A value of k_3 for the sar-34 RNA–ant RNA pairing reaction is not given (na) because the step corresponding to k_3 does not occur.

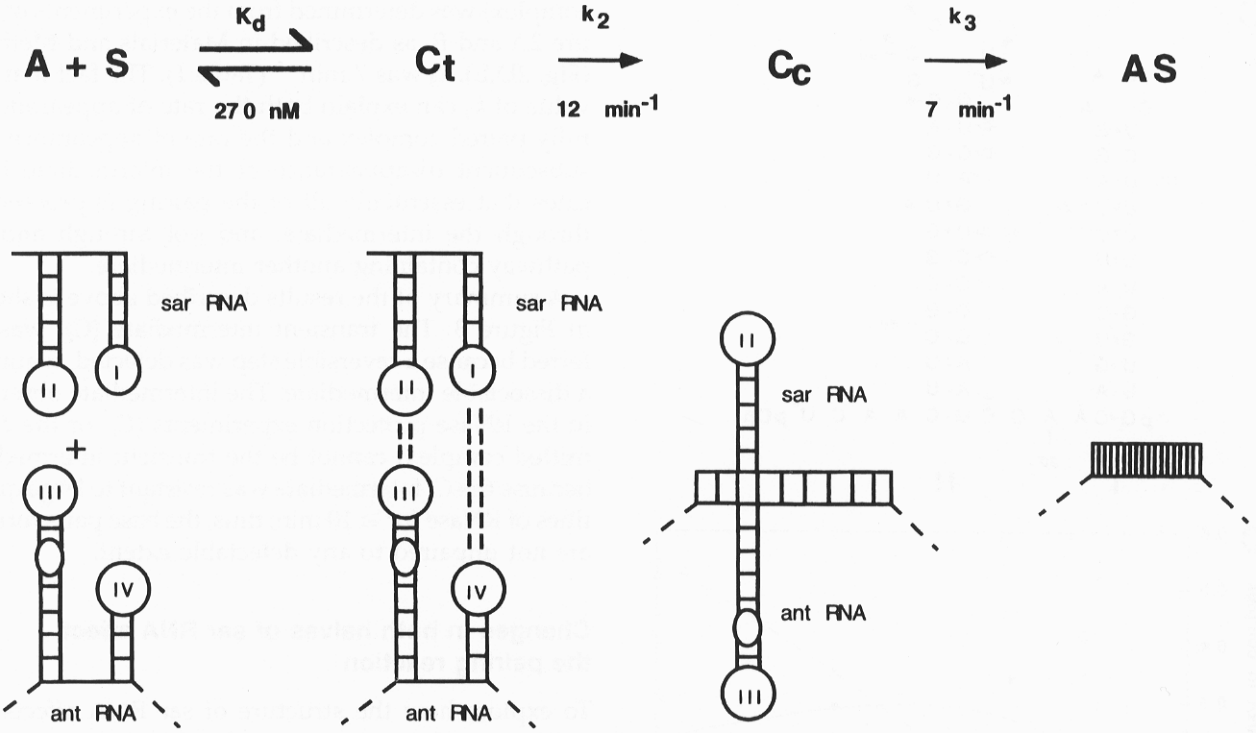

FIGURE 3. Schematic representation of the sar RNA–ant RNA pairing pathway. Sar RNA and ant RNA secondary structures and the numbering of the hairpins are described in Schaefer and McClure (1996). Solid lines represent stable base pairs; dashed lines represent reversible base pairs. Descriptions of the pairing pathway and the structures of the intermediates are given in the text.

mutation changed the pairing reaction only slightly. The strength of the initial interaction was increased 1.4-fold, but k_2 was also reduced by 1.5-fold, resulting in an overall selectivity (k_2/K_d) similar to that seen in the wild-type pairing reaction. The 13C → U mutation affected the pairing reaction more strongly. The strength of the initial interaction was increased 2.5-fold, but k_2 was reduced 6-fold, resulting in a 2.6-fold reduction in overall selectivity.

To further explore how the structure of sar RNA affects the pairing reaction, we measured the (composite rate constant) k_{obs} corresponding to formation of the fully paired complex for sar RNAs with 5′ or 3′ truncations, using the RNase protection assay. Populations of 5′ end-labeled sar RNAs with 3′ truncations of varying length or 3′ end-labeled sar RNAs with 5′ truncations of varying length were produced by limited alkaline hydrolysis of sar RNA. These mixtures of shortened sar RNAs were incubated with excess ant RNA, and the rate of appearance of each RNA fragment (corresponding to an individual truncation variant) was used to calculate k_{obs} values for the shortened sar RNA–ant RNA reactions.

The effect of sar RNA 3′ truncations on k_{obs} (Fig. 5A,C) indicates that sequences in the second half of sar RNA are definitely required for some step in pairing. Elimination of nt 67 and 68 from the 3′ tail caused a 25–150-fold reduction in k_{obs}; the additional removal of nt 66 caused a still greater reduction. Interestingly, after the 3′ tail was totally removed, the value of k_{obs} was equivalent to the wild-type value. Nucleotides 56–65 could be removed from the 3′ half of stem II without affecting the value of k_{obs}, indicating that the entire stem is not required for pairing. However, after nt 55 was removed, and the sar RNA stem II was presumably no longer present, the pairing rate was reduced 25–150-fold. Removal of additional nucleotides did not cause a further decrease in pairing rate. Therefore, loop sequences as well as the loop per se are probably required for optimal pairing. The drastic reduction in k_{obs} seen with the 57 nt sar RNA is intriguing. Sar RNA structure modeling using the MULFOLD (v. 2.0) RNA folding program (Jaeger et al., 1989a, 1989b; Zuker, 1989) did not indicate any alternative structures formed in the 57 nt sar RNA.

The effect of sar RNA 5′ truncations on k_{obs} (Fig. 5B,C) indicates that sequences in the first half of sar RNA are also required for wild-type pairing. When nt 1–27 were removed, a greater than 150-fold decrease in k_{obs} was observed, indicating that hairpin II, by itself or in conjunction with the interhairpin region, has a severely reduced ability to pair. Interestingly, k_{obs} was within 2.5-fold of the wild-type value (data not shown) after nt 1–43 were removed.

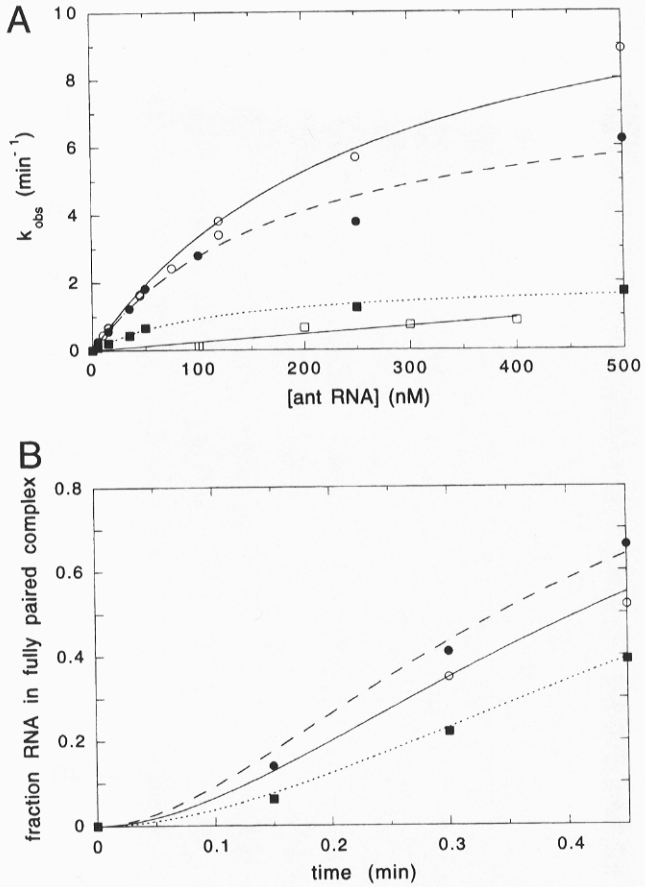

FIGURE 4. Effect of sar RNA mutations and truncations on pairing kinetics. Gel-shift and RNase A protection experiments were performed and analyzed as described in the legends of Figures 1 and 2. RNase protection experiments contained 5′ end-labeled sar RNAs and 182 nM (12U → A) or 352 nM (13C → U) ant RNA. **A:** Determination of K_d and k_2. k_{obs} values for sar RNA mutant 12U → A (●, dashed line), sar RNA mutant 13C → U (■, dotted line), and sar RNA truncation sar-34 (□, solid line) are plotted versus ant RNA concentration. For comparison, the data of Figure 1 (wild-type sar RNA) (○, solid line) are shown. Linear least-squares fits (Equation 3 in Materials and Methods) are indicated by the lines; numerical values are given in Table 1. **B:** Determination of k_3. The fraction of the RNA in the fully paired complex is plotted versus time for sar RNA mutant 12U → A (●, dashed line) and sar RNA mutant 13C → U (■, dotted line). Indistinguishable values were obtained when k_3 was determined from the kinetics of the intermediate and of the fully paired duplex; thus, only data corresponding to appearance of the fully paired duplex are displayed. For comparison, data from Figure 2A (wild-type sar RNA) (○) are shown. Fits (Equations 4 and 5 in Materials and Methods) are indicated by the lines. k_3 (12U → A) is 6.4 min^{-1}; k_3 (13C → U) is 8.1 min^{-1}. At t = 2.5 min, the fraction of RNA in the intermediate complex had reached 0 and the fraction of RNA in the fully paired complex had reached 1.0.

The pairing reaction is Mg^{2+}-dependent

The results of earlier studies indicated that the sar RNA-ant RNA pairing reaction is Mg^{2+}-dependent (Liao, 1988). The experiments of Figure 6 examine the dependence of k_{obs} on Mg^{2+}. A plot of normalized k_{obs} (see Materials and Methods) versus Mg^{2+} concentration was sigmoidal, showing that more than one Mg^{2+} ion is required for a maximal pairing rate. k_{obs} at saturating concentrations of Mg^{2+} (1.3 min^{-1} – 1.9 min^{-1}) was 100–200-fold increased over the rate in the absence of Mg^{2+}. The Hill coefficient (n = the apparent number of Mg^{2+} ions acting cooperatively in the reaction) was 1.5; $Mg_{1/2}$ (the concentration of Mg^{2+} at half-maximal k_{obs}) was 6.1 mM.

Several RNA structures could account for the Mg^{2+}-dependence of the pairing reaction

The pairing reaction initiates with formation of reversible contacts between sar RNA and ant RNA loop nucleotides, followed by concomitant unwinding of sar RNA and ant RNA hairpin stems and duplex propagation. Sar RNA and ant RNA structures are Mg^{2+}-dependent (Schaefer & McClure, 1996); the Mg^{2+}-dependence of the pairing reaction presumably reflects the requirement for Mg^{2+} to stabilize RNA structure(s) that promote these step(s). Specifically, Mg^{2+} could be stabilizing (1) one or more secondary structures required for formation of loop(s) involved in the initial interaction, (2) tertiary structures required to present the loop structure(s) in a particular conformation, or (3) particular secondary or tertiary structure(s) that favor hairpin unwinding. In addition, Mg^{2+} could be stabilizing the initial base pairs formed between the loops.

In order to distinguish between these possibilities, we compared the Mg^{2+}-dependent structure formation results (Schaefer & McClure, 1996) with the Mg^{2+}-dependence of pairing examined in the experiments of Figure 6. Mg^{2+}-dependent structure formation was assayed by measuring the ability of Mg^{2+} to inhibit ss-specific RNase cleavage. We assume that the concentration of Mg^{2+} that half-maximally inhibited cleavage is equal to the concentration of Mg^{2+} that half-maximally promoted structure formation (K_{Mg}). The K_{Mg} values were compared to the Mg^{2+}-dependence of pairing in the following way. Because the Hill coefficient (n) was 1.5, more than one Mg^{2+} ion is required for pairing. Thus, the $Mg_{1/2}$ and n values obtained from the experiment of Figure 6 were related to the individual dissociation constants K_1 and K_2 for binding of Mg^{2+} to particular RNA structures using the Adair equation describing binding of two ligands (see Materials and Methods). The results of this analysis indicated the presence of a high-affinity and a low-affinity site: K_1 was 30 ± 20 mM and K_2 was 2 ± 1 mM.

A comparison of the K_1 and K_2 values with the K_{Mg} values (Fig. 7) indicates that the Mg^{2+}-dependence of pairing can be explained in terms of a requirement for stabilization of individual RNA structures. The K_1 value is similar to the K_{Mg} value for formation of tertiary structure involving sar RNA loop II (compare K_{Mg} at sar RNA nt 45 and 47 with K_1; see Schaefer & McClure, 1996 for a discussion of the interpretation of specific RNase digestion sites). Several K_{Mg} values similar to K_2 are observed. First, the K_{Mg} values observed for

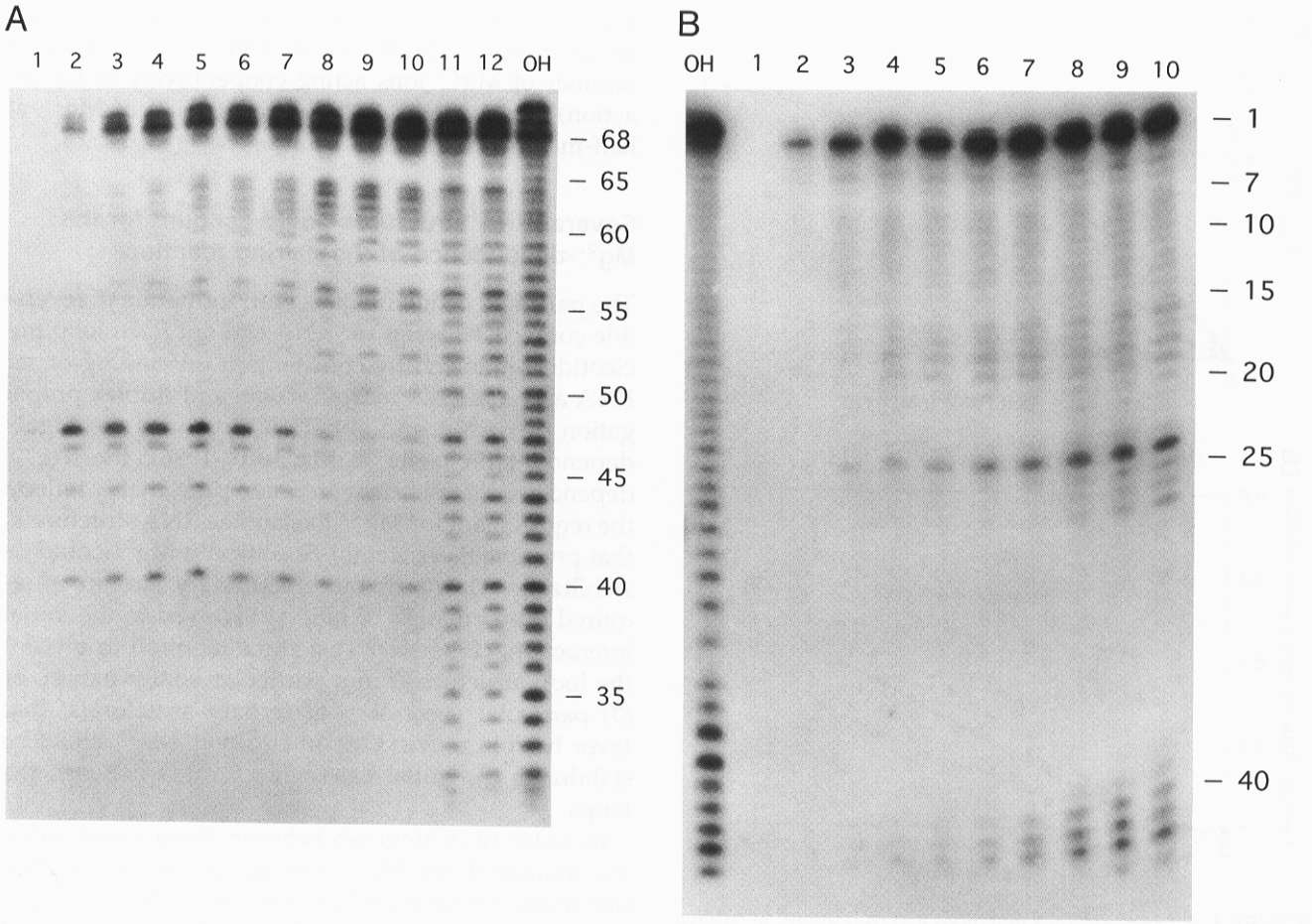

FIGURE 5. Effect of sar RNA truncations on k_{obs}. Sets of 5′ or 3′ end-labeled sar RNAs varying in length from 1 to 68 nt were made using limited alkaline hydrolysis. These RNAs were used in RNase protection experiments that were performed and analyzed as described in the legend of Figure 2. OH, control lane with no added RNase. Numbers next to the bands indicate the 3′ (part A) or 5′ (part B) terminal sar RNA nucleotide. **A:** Autoradiograph from a RNase protection experiment using 5′ end-labeled hydrolysis products and 15 nM ant RNA. RNA fragments had nucleotides removed from the 3′ end. Time points (min) are (from 1–12) 0, 0.2, 0.35, 0.55, 0.7, 0.9, 1.5, 3, 5.5, 7, 30, and 30.5 min. **B:** Autoradiograph from an RNase protection experiment using 3′ end-labeled hydrolysis products and 20 nM ant RNA. RNA fragments had nucleotides removed from the 5′ end. Time points (min) are (from 1–10) 0, 0.4, 0.8, 1, 1.2, 2, 3, 10, 15, and 40 min. **C:** A schematic representation of the results of experiments like those of A and B. Top panel illustrates the change in k_{obs} when nucleotides were removed from the 3′ end of sar RNA. RNAs ending in nucleotides shown as bold (≤5-fold), shadowed (25–150-fold), or underlined (>150-fold) had the indicated reductions in k_{obs}. The magnitude of the reduction in k_{obs} denoted by underlined nucleotides is a lower estimate because no detectable pairing occurred over the time course of the reaction. The k_{obs} for RNAs ending in nucleotides shown in plain font was not examined. Bottom panel shows the change in k_{obs} when nucleotides were removed from the 5′ end of sar RNA (3′ end-labeled sar RNA), using the same conventions as in the top panel, except that the highlighted nucleotide indicates the 5′ terminal nucleotide. For pairing rates close to the wild-type rate, the standard deviation in k_{obs} was generally ≤ 30%.

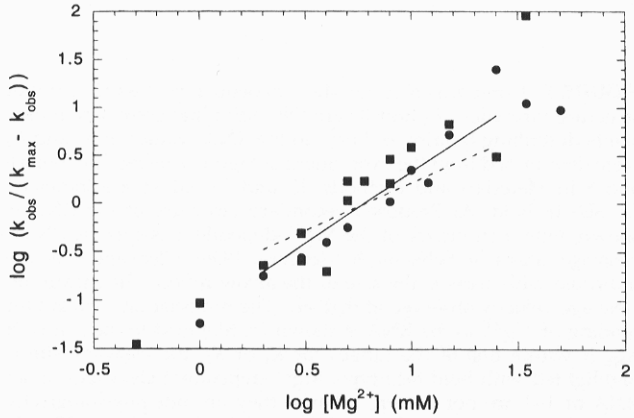

FIGURE 6. Mg^{2+} dependence of the sar RNA-ant RNA pairing reaction. Pairing reactions were performed in the presence of the indicated concentration of Mg^{2+} and analyzed as described in the legend of Figure 1. Data are plotted as a Hill plot (logarithmic form of Equation 6 in Materials and Methods). Results of two experiments with different maximum k_{obs} values (k_{max}) are shown, using different symbols. In experiment 1 (■), k_{max} was 1.3 min^{-1}; in experiment 2 (●), k_{max} was 1.9 min^{-1}. The solid line indicates the fit: $Mg_{1/2}$ is 6.1 ± 0.9 mM and n = 1.5 ± 0.2. For comparison, a hyperbolic curve (n = 1) with the same $Mg_{1/2}$ is indicated by the dashed line. A least-squares fit using Equation 3 (n = 1) in Materials and Methods gave K_{Mg} = 30 ± 20 mM; thus, the Hill plot parameters were used to describe the Mg^{2+}-dependence.

formation of sar RNA tertiary structure involving loop I (cleavage at nt 13, 14, and possibly 22) or the inter-hairpin region (cleavage at nt 31 and 32) are similar to the K_2 value. Second, the K_{Mg} for cleavage at nt 109 in ant RNA loop IV (K_{Mg} = 2 ± 1 mM) is in the correct range to explain K_2. However, it is not likely that stabilization of this structure corresponds to K_2, because cleavage at the pairing partner of nt 109 (nt 99) has a K_{Mg} value of 0.8 ± 0.1 mM, indicating that the K_{Mg} for formation of this hairpin is probably, in fact, less than 1 mM. Finally, the K_{Mg} values for formation of one or more (as yet unidentified) tertiary interactions in ant RNA (cleavages at 7, 65, 85, 87, 89, 102, and 112–132) are also similar to K_2. These results indicate that the Mg^{2+}-dependence of pairing can be explained in terms of stabilization of individual RNA structures, although a specific assignment of the high-affinity site cannot be made. However, these results do not by themselves prove that the Mg^{2+}-dependence of pairing is the result of a requirement for stabilization of individual RNA structures, because the Mg^{2+} ions could be stabilizing the initial complex between the two RNAs.

Both Mg^{2+} ions are probably stabilizing tertiary structures

In order to further investigate the nature of the Mg^{2+} binding requirement, we examined the ability of other divalent cations and polyamines to substitute for Mg^{2+}. The cationic specificity of the reaction can be used to probe the nature of the Mg^{2+}-binding sites because the stabilization of secondary structure and the stabilization of tertiary structure are expected to exhibit different specificites. Hairpin helices can be stabilized by any positively charged cation. In contrast, stabilization of tertiary structure sometimes involves specific coordination of the cations to the RNA; thus, the identity of the cation can affect its ability to support tertiary structure (Teeter et al., 1981; Liang et al., 1994). Therefore, if one or more of the Mg^{2+} ions involved in the pairing reaction is stabilizing tertiary structure, it is expected that the pairing reaction will exhibit cationic specificity.

An initial survey of the ability of various divalent cations and polyamines to substitute for Mg^{2+} in the pairing reaction was done by determining k_{obs} at 15 nM ant RNA over a range of cation concentrations (Schaefer, 1996). At 10 mM cation, Ca^{2+} and Mn^{2+} had k_{obs} values within 80% of that observed with Mg^{2+}; Sr^{2+} had a k_{obs} value approximately 20% of that observed with Mg^{2+} (Schaefer, 1996); and Co^{2+} and Zn^{2+} had k_{obs} values less than 10% of that observed with Mg^{2+} (data not shown). The effect of the polyamine spermine (4^+) on k_{obs} (Fig. 8) was similar in magnitude to the effect of Mg^{2+}; however, the concentration dependence was hyperbolic. This result suggests either that one spermine can substitute for two Mg^{2+} ions or that two spermines are binding with the same affinity at each site. Although spermine was able to substitute for Mg^{2+}, neither the polyamines spermidine (3^+), putrescein (2^+), nor high concentrations of K^+ (data not shown) were able to substitute for Mg^{2+}.

Those divalent cations or polyamines that exhibited k_2 values similar (±2-fold) to that observed with Mg^{2+} in the above assay were examined further. K_d and k_2 values were measured in the presence of 10 mM divalent cation or polyamine. The results were compared to the values of K_d and k_2 obtained in the presence of 10 mM Mg^{2+} (Table 2). Although Mn^{2+}, Ca^{2+}, or spermine stimulated pairing significantly, the values of K_d and/or k_2 obtained were different than those obtained with Mg^{2+}. Mn^{2+} and Ca^{2+} actually promoted pairing better than Mg^{2+}. In the presence of Mn^{2+}, k_2 was increased 60%. In the presence of Ca^{2+}, k_2 was increased only 20%; however, the affinity of the initial interaction was increased 30%, causing an overall increase in the rate of formation of the first stable complex. In the presence of spermine, the overall rate of formation of the first stable complex was the same as in the presence of Mg^{2+}; however, this result was achieved by compensatory changes in K_d and k_2. The affinity of the initial interaction was increased 60%, whereas k_2 was reduced 50%.

The experiments of Figure 8 and Table 2 indicate that the pairing reaction exhibits cationic specificity. The fact that the pairing reaction exhibits cationic specificity suggests that at least one of the Mg^{2+} ions is binding to a site that has specific size or coordination requirements. Because ion binding to hairpins does

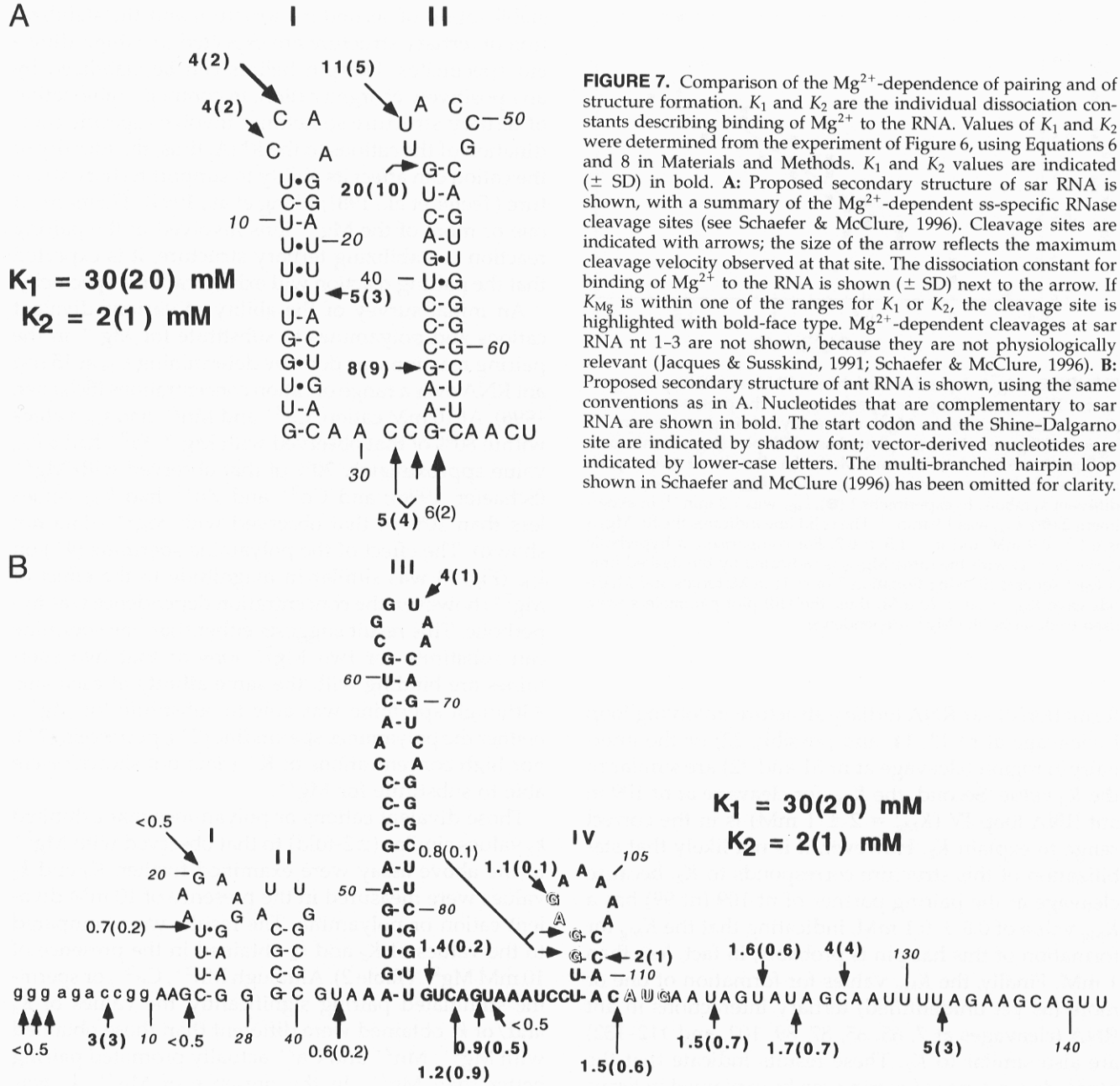

FIGURE 7. Comparison of the Mg^{2+}-dependence of pairing and of structure formation. K_1 and K_2 are the individual dissociation constants describing binding of Mg^{2+} to the RNA. Values of K_1 and K_2 were determined from the experiment of Figure 6, using Equations 6 and 8 in Materials and Methods. K_1 and K_2 values are indicated (± SD) in bold. **A:** Proposed secondary structure of sar RNA is shown, with a summary of the Mg^{2+}-dependent ss-specific RNase cleavage sites (see Schaefer & McClure, 1996). Cleavage sites are indicated with arrows; the size of the arrow reflects the maximum cleavage velocity observed at that site. The dissociation constant for binding of Mg^{2+} to the RNA is shown (± SD) next to the arrow. If K_{Mg} is within one of the ranges for K_1 or K_2, the cleavage site is highlighted with bold-face type. Mg^{2+}-dependent cleavages at sar RNA nt 1-3 are not shown, because they are not physiologically relevant (Jacques & Susskind, 1991; Schaefer & McClure, 1996). **B:** Proposed secondary structure of ant RNA is shown, using the same conventions as in A. Nucleotides that are complementary to sar RNA are shown in bold. The start codon and the Shine–Dalgarno site are indicated by shadow font; vector-derived nucleotides are indicated by lower-case letters. The multi-branched hairpin loop shown in Schaefer and McClure (1996) has been omitted for clarity.

not involve size or coordination requirements (Teeter et al., 1981; Liang et al., 1994), the Mg^{2+} is probably binding to a tertiary structure rather than to a hairpin. We refer to this site as "site A." In order to determine if the other Mg^{2+} binding site (referred to as "site B") also has cationic specificity, we examined the dependence of k_{obs} on Mg^{2+} in the presence of polyamines that did not by themselves stimulate pairing significantly (spermidine and putrescein). If site A has cationic specificity but site B does not, it is expected that polyamines should be able to bind at site B, causing the shape of the Mg^{2+}-saturation curve to be hyperbolic rather than sigmoidal, with a k_2 value comparable to that obtained with Mg^{2+} alone. This prediction was tested in the experiment of Figure 9. The Mg^{2+}-dependence of pairing in the presence of spermidine or putrescein was hyperbolic, suggesting that polyamines can bind to site B and stimulate pairing. However, the value of k_2 obtained in the presence of polyamine was twofold less than that in the presence of Mg^{2+} alone. Thus, the polyamine was acting as a noncompetitive inhibitor. We suggest that the binding of the polyamine at a site (presumably at or near site B) is able to stimulate pairing to some extent, but also prevents Mg^{2+} from binding to site B. Because the binding of polyamine at or near site B is detectably different than binding of Mg^{2+} to site B, site B also must exhibit some cationic specificity. Therefore, the

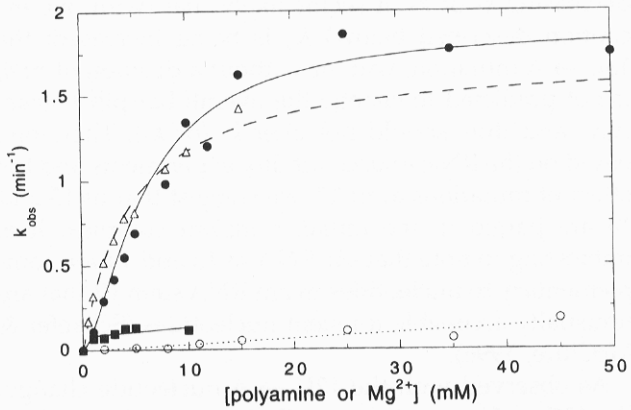

FIGURE 8. Ability of polyamines to substitute for Mg^{2+} in the pairing reaction. Gel-shift experiments were performed as described in the legend of Figure 1, in the presence of the indicated concentrations of polyamines. **A:** k_{obs} when Mg^{2+} was replaced by spermine (△, dashed line), spermidine (■, solid line), or putrescein (○, dotted line) is plotted versus ant RNA concentration. For comparison, the Mg^{2+}-dependence data from experiment 2 of Figure 6 (●) are shown. The best fit of the Mg^{2+}-dependence data (Fig. 6) is indicated with the solid line. Dashed line corresponds to the values of K_d (4.7 ± 0.4 mM) and k_2 (1.7 ± 0.4 min^{-1}) determined using Equation 3 in Materials and Methods. Other lines indicate simple linear least-squares fits.

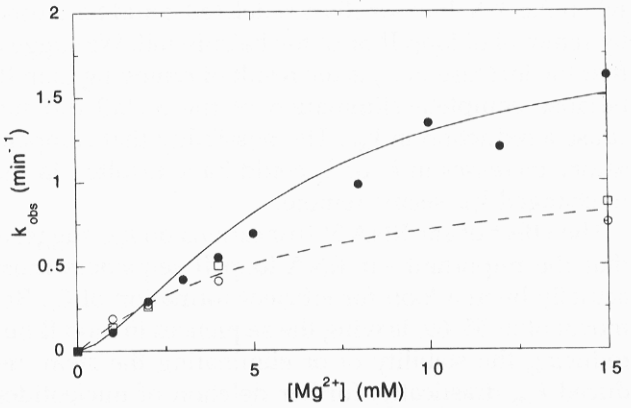

FIGURE 9. Mg^{2+}-dependence of the pairing reaction in the presence of 10 mM putrescein or spermidine. k_{obs} in the presence of putrescein (□) or spermidine (○) is plotted versus Mg^{2+} concentration. For comparison, the Mg^{2+} dependence data from experiment 2 of Figure 6 (no polyamine) (●) are shown. Gel-shift experiments were performed and analyzed as described in the legend to Figure 1, in the presence of 10 mM polyamine and the indicated concentrations of Mg^{2+}. Dashed line indicates the linear least-squares fit (Equation 3 in Materials and Methods) of the Mg^{2+}-dependence data (+ polyamine): K_d is 4 ± 1 mM; k_2 is 0.9 ± 0.2 min^{-1}. Solid line indicates the best fit to the Mg^{2+}-dependence data (from Fig. 6) (no polyamine): $Mg_{1/2}$ is 6.1 ± 0.5 mM; k_2 is 1.9 min^{-1}. The only way the (+ polyamine) data can be fit to a sigmoidal curve like that for the (− polyamine) data is if the k_{obs} values at 15 mM Mg^{2+} point are off by approximately twofold. This is extremely unlikely, because the error in the gel-shift measurements is less than 10% (for instance, see Fig. 1C).

Mg^{2+} binding site B is also probably involved in stabilizing tertiary structure.

DISCUSSION

The pairing mechanism

We propose the following pathway to describe the pairing of sar RNA to ant RNA:

$$A + S \overset{K_d}{\rightleftharpoons} C_t \overset{k_2}{\longrightarrow} C_c \overset{k_3}{\longrightarrow} AS,$$

based on the following observations. First, a plot of k_{obs} (ant RNA in excess) versus ant RNA concentration was hyperbolic. Thus, the first step is reversible. Second, a stable intermediate resistant to large quantities of RNase (C_c) was observed, defining the step described by k_3. Third, the presence of a transient complex (C_t) was inferred from the fact that C_c cannot be the form in equilibrium with the free RNAs because C_c was stable to large quantities of RNase A. It should be noted that, because the sar RNA used in the RNase protection experiments was end-labeled, we cannot detect intermediates that are not paired at least at one end. Thus, it is possible that the pairing reaction proceeds through additional stable intermediates before the observed intermediate forms.

Pairing of sar RNA to ant RNA proceeds through formation of an initial, transient complex, followed by stable duplex formation. We discuss the nature of the transient intermediate and the process of stable duplex formation below.

TABLE 2. Effect of divalent ion substitutions on the binding and propagation steps of the pairing reaction.[a]

Cation added	K_d (nM)	k_2 (min^{-1})	k_2/K_d (M^{-1} s^{-1})
10 mM Mg^{2+}	270 (30)	12 (1)	7.6×10^5
10 mM Mn^{2+}	260 (20)	19 (2)	1.2×10^6
10 mM Ca^{2+}	200 (20)	14 (1)	1.1×10^6
10 mM spermine	120 (30)	6 (2)	8.3×10^5
None	≫500	nd	7.3×10^3

[a]Gel-shift experiments were performed and analyzed as described in the legend of Figure 1, in the presence of 10 mM divalent cation or spermine. Standard deviations are given in parentheses. Values in the presence of Mg^{2+} are repeated from Table 1. nd, not determined.

The transient intermediate

The effect of removing the 3′ half of sar RNA on K_d suggests that nucleotides in sar RNA loop II are involved in the initial complex (C_t). Removal of sar RNA nt 34–68, including hairpin II and the 3′ tail, caused a significant increase in K_d without altering any of the structure in hairpin I (Schaefer & McClure, 1996). Thus, some sequences in the 3′ half of sar RNA must be important for formation of C_t.

Assuming that initial contacts take place between single-stranded regions, the increase in K_d observed

when the 3′ half of sar RNA is deleted could be caused by removal of loop II or of the hairpin tail. We suggest that the increase in K_d is the result of removing loop II, because complete elimination of the 3′ tail did not cause a reduction in k_{obs}. The possibility that compensatory increases in k_2 or k_3 could have resulted in the unchanged k_{obs} seems remote.

The effect of sar RNA 3′ truncations on k_{obs} suggests that the important sar RNA loop II sequences must actually be in a loop for efficient formation of C_t. Removal of nt 55–69, leaving the sequences in loop II but reducing the stability of or eliminating the stem, reduced k_{obs} drastically; further deletion of nucleotides in the loop did not cause an additional decrease in k_{obs}. The reduction in k_{obs} was probably the result of an increase in K_d. This hypothesis is supported by the observation that one of the Mg^{2+} ions required for pairing is probably involved in stabilizing tertiary structure involving sar RNA loop II. Again, however, we cannot exclude the possibility that k_2 or k_3 was reduced.

Sar RNA nt 12 is not paired in C_t. Disruption of a putative loop–loop U-A base pair with an A/A mismatch at nt 12 (mutation 12U → A) actually increased the affinity of the initial interaction, indicating that this nucleotide is not itself paired in C_t. However, the fact that the value of K_d was changed suggests that the mutation affects formation of C_t in some way. The 12U → A mutation changes sar RNA structure in two ways (Schaefer & McClure, 1996). The top base pair in hairpin I is disrupted by the mutation, and the tertiary structure involving loop II is altered. Thus, the increase in affinity could be the result of a more favorable loop conformation in either or both of the loops. Loop structure effects are probably also seen in another pairing reaction. The strength of reversible base pairs formed in the pairing between model hairpins derived from the Col E1 RNA I and RNA II is affected both by the composition of the loops and the stems; NMR analysis indicates that the loop–loop complex stacks on the hairpin stems (Eguchi & Tomizawa, 1991; Gregorian & Crothers, 1995; Marino et al., 1995). Thus, it is likely that the precise structures both of the individual loops and the complex formed between them affect the strength of the initial complex.

Two observations suggest that sar RNA nt 13 and 14 are paired in C_t. First, during the sar RNA–ant RNA pairing reaction, susceptibility to the ss-specific RNase A at nt 13 and 14 disappeared before susceptibility at nt 2 disappeared. This result suggests that an initial step involves pairing at nt 13 and 14 (Liao, 1988). Second, a number of mutations at nt 13 impair the pairing reaction. Changing nt 13 from C → A caused a fivefold reduction in k_{obs} by itself or in combination with a mutation that eliminates nt 4; changing nt 13 from C → U also caused a fivefold reduction in k_{obs}. Although the nt 13 mutations could be increasing K_d or decreasing k_2 or k_3, it seems likely that (with one exception described below) K_d is being increased: the 13C → A mutation, with or without a deletion of nt 4, is not predicted to change the overall hairpin I structure, and thus should not alter k_2 (or k_3). Therefore, based on the RNase susceptibility experiments and the effect of mutations at nt 13, we suggest that nt 13 and 14 are paired in the initial, transient complex. It is interesting to note that sar RNA nt 13 and 14 are complementary to nucleotides in ant RNA stem IV that are unusually accessible for stem nucleotides (Schaefer & McClure, 1996).

As observed with the 12U → A nucleotide change, the 13C → U mutation actually increases the strength of the initial interaction. The increase in affinity is thus probably a result of altered secondary or tertiary structure. The 13C → U mutation reduces the size of loop I, by making a 3-nt U turn possible (Schaefer & McClure, 1996). In addition, the mutation changes the tertiary structure in loop II. Either change or both changes together could cause the increased affinity. Although the intermolecular C-G base pair was replaced by a U•G base pair, the complex strength increased. This observation suggests that the magnitude of the increase in affinity caused by the changed loop structure is sufficient to overcome the energetic loss associated with the nucleotide change as well as to cause a further observable increase in affinity.

Many sar RNAs with 5′ truncations that eliminate nt 13 and 14 paired to ant RNA with k_{obs} values within fivefold of wild-type, apparently contradicting the idea that formation of C_t requires pairing at nt 13 and 14. We propose that sar RNAs lacking nt 13 and 14 are able to pair at wild-type or near wild-type rates because alternative pairing pathways can be adopted when the 5′ sar RNA sequences are no longer contained in a hairpin. In this model, the effects of 5′ truncations can be grouped into three classes. The first class involves removal of only a few nucleotides and does not disrupt stem I. The pairing pathway in this case is identical to the wild-type one, and initial contacts are not affected; k_{obs} is within fivefold of the wild-type value. In the second class of truncations, enough nucleotides are removed to disrupt stem I and thus leave a long, single-stranded region. RNA–RNA pairing bypasses the loop–loop interaction step, and stable complex formation initiates between single-stranded sar RNA nucleotides and ant RNA loop nucleotides either in loop IV or in the multi-branched loop, depending on the length of the sar RNA truncation. Again, this alternative pathway results in k_{obs} values within fivefold of the wild-type value. The third class involves deletion of so many nucleotides (deletion of at least nt 1–25) that the sar RNA single-stranded region is very short, and a helix long enough to be stable is not formed before a pause in helix propagation corresponding to unwinding of sar RNA stem II and ant

RNA stem III occurs. These RNAs are severely hampered in pairing (k_{obs} is reduced > 25-fold) because they cannot form C_t (loop I is gone) and cannot initiate stable complex formation through another pathway.

The initial complex C_t almost certainly involves only loop–loop interactions. Initial base pairs can form only between single-stranded nucleotides. Aside from the loops, sar RNA contains only one single-stranded region: the interhairpin region. The interhairpin region is complementary to a region in ant RNA that is paired (Schaefer & McClure, 1996). Therefore, initial contacts are presumably being made only between nucleotides in complementary loops.

The number of base pairs formed in the initial complex (C_t) was estimated roughly from the value of K_d. The result suggests that a small number of reversible base pairs form involving nucleotides in each sar RNA loop. The observed K_d value of 270 (± 30) nM for formation of the initial complex corresponds to $\Delta G^\circ = -9.4$ (± 0.1) kcal/mol. Because the ΔG° values for formation of base pairs are sequence specific (Freier et al., 1986), any estimate of the number of base pairs depends on the assumptions made about the base composition of the paired region. Because nucleation in oligomers takes place preferentially at G-C base pairs (Cantor & Schimmel, 1980), we assumed that nucleation between nucleotides in sar RNA loop II and their complements in ant RNA loop III occurs at G-C base pairs. Thus, we assume that sar RNA nt 49, 50, and 51 are paired in the initial complex. In addition, the evidence discussed above indicates that sar RNA nt 13 and 14 are paired in the initial complex. The minimum complex with these nucleotides paired has a predicted ΔG° value of −7.8 kcal/mol. This is on the order of the observed ΔG° value, indicating that only 2–4 nt in each sar RNA loop form base pairs in C_t. Because at least some short duplexes formed between nucleotides in loops are more stable than the same duplexes formed between nonloop nucleotides (Grosjean et al., 1976; Eguchi & Tomizawa, 1991; Gregorian & Crothers, 1995), the number of base pairs estimated using the standard ΔG° values may be an overestimate.

The propagation steps

Two kinetically distinguishable propagation steps were observed. In the first step, nt 1–32 of sar RNA (hairpin I and the interhairpin region) and nt 65–68 (the 3′ tail) pair to ant RNA nucleotides. The pairing requires the disruption of sar RNA hairpin I and its complement, as well as the four bottom base pairs of ant RNA stem III. In the next step, all remaining stems (the rest of ant RNA stem III and sar RNA stem II) unwind and complete duplex formation occurs.

Topological constraints dictate that the intermediate complex (C_c) cannot form with the simultaneous unwinding of sar RNA stem I and ant RNA stem IV and propagation of the short, transient helix formed between sar RNA loop I and ant RNA loop IV as the stems unwind. Therefore, stable complex formation must initiate either (1) between sequences that are single-stranded in one RNA and contained in a loop in the other RNA or (2) between sequences that are single-stranded in both RNAs. Although it is formally possible that stable complex formation could initiate from the initial sites of contact in sar RNA loop I and its complement if the stems were disrupted completely before intermolecular helix propagation began, the magnitude of the activation energy estimated from the temperature dependence of k_{obs} ($E_a \approx 17$ kcal/mol; (Schaefer, 1996)) suggests that this process does not occur.

Stable complex formation is not initiating between a single-stranded sequence and a loop sequence. An examination of the proposed structures of ant RNA and sar RNA (see Schaefer & McClure, 1996) reveals no complementary sequences that are single-stranded in one RNA and in a loop in the other RNA. Other than ant RNA loops III and IV, the only ant RNA single-stranded sequence is in the multi-branched loop. The sar RNA sequence complementary to the multi-branched loop sequence is in stem I. Therefore, pairing cannot be initiating between these two regions.

Stable complex formation is probably initiating between the sar RNA interhairpin region and the 3′ end of ant RNA stem III. The only unambiguously identified nonloop, single-stranded region in sar RNA is the interhairpin region. The interhairpin region is complementary to the last 4 nt in ant stem III; however, the bottom of this stem is accessible to a ss-specific RNase at least some of the time (Schaefer & McClure, 1996). Thus, pairing is probably initiating between nucleotides in the sar RNA interhairpin region and the bottom of ant RNA stem III during that fraction of the time that ant RNA stem III sequences are accessible. Although the bottom of ant RNA stem III is accessible some fraction of the time and is complementary to the sar RNA 3′ tail, stable complex formation is not initiating between these regions. In free sar RNA, the 3′ tail is clearly inaccessible to ss-specific RNases (Schaefer & McClure, 1996). In addition, complete deletion of the sar RNA 3′ tail does not affect k_{obs}, indicating that the 3′ tail is not required for pairing.

Sar RNA mutations 12U → A and 13C → U cause a reduction in the value of k_2. The observed reductions in k_2 cannot be explained by postulating that stable complex formation occurs only when sar RNA hairpin I is completely unwound, and that the value of k_2 reflects the proportion of time that the hairpin is unwound. The predicted ΔG° values for the wild-type and mutant sar RNA hairpins suggest that the RNA is found in hairpin form > 99% of the time at 37 °C; the absence of ss-specific RNase digestion at most nucleotides in stem I in both the wild-type and mutant sar RNAs (see Schaefer & McClure, 1996) is consistent with

this prediction. In addition, the activation energy for the k_2 step measured with wild-type sar RNA (see above) indicates that total unwinding of hairpin I does not occur before stable complex formation. Therefore, the observed differences in k_2 do not reflect the fraction of time that the hairpin is unwound. Thus, the mutations must decrease the rate of unwinding of one or more base pairs. Presumably, the change in structure introduced by the mutations stabilizes one or more base pairs so that the total enthalpy for disrupting the base pair(s) is greater. The change in k_2 observed with subtle changes in the sar RNA hairpin I is similar to observations made in the copA RNA–copT RNA pairing reaction: removal of bulged nucleotides and internal loops, or even moving these elements, had a marked effect on the rate of hairpin disruption (Hjalt & Wagner, 1995).

Structures that are required for maximal pairing rates

The pairing of sar RNA to ant RNA is strongly Mg^{2+}-dependent. The shape of the Mg^{2+}-dependence curve indicates that binding of at least two Mg^{2+} ions is required for maximal k_{obs} values. The dissociation constants for binding of Mg^{2+} to the high- and low-affinity sites, respectively, are around 2 mM and 30 mM.

The Mg^{2+}-dependence of the pairing reaction presumably reflects a requirement for Mg^{2+} to stabilize RNA structure(s) that promote pairing. We argue that the two observed Mg^{2+} ions are involved in stabilization of RNA tertiary structure, for the following reasons. First, the pairing reaction exhibited cationic specificity. Therefore, at least one of the Mg^{2+} ions binds to a site (site A) that has specific size or coordination requirements. This finding is most consistent with the suggestion that Mg^{2+} binding at site A stabilizes tertiary structure. Second, the shape of the Mg^{2+}-dependence curve in the presence of those polyamines that did not themselves stimulate pairing became hyperbolic with a k_2 twofold less than that observed with Mg^{2+} alone. This result suggests that the polyamines are able to bind to a second site (site B) and stimulate pairing to some extent, but that the binding of polyamine to site B is not as effective at promoting pairing as is the binding of Mg^{2+} to site B. The fact that the value of k_2 was twofold less when polyamines were bound to site B than when Mg^{2+} was bound to site B suggests that this site may also have some specific size or coordination requirements. Again, this finding is most consistent with Mg^{2+} binding at site B, supporting tertiary structure. Thus, both Mg^{2+} ions are most likely involved in stabilization of tertiary structure.

The requirement for appropriate tertiary structure may be unusual in antisense RNA–target RNA pairing reactions. Mutations that totally eliminate the antisense RNA hairpin but that do not change the nucleotides in the region of initial interaction have no effect on the RNA•OUT–RNA•IN pairing reaction (Kittle et al., 1989). This observation suggests that the precise structure of the antisense RNA is not important (the target RNA is unstructured in the region of interaction). Similarly, individual RNA tertiary structures are probably not required for maximal pairing rates in the copA RNA–copT RNA pairing reaction. The pairing reaction is Mg^{2+}-dependent; however, the Mg^{2+} requirement can be met by high concentrations of monovalent ion (Persson et al., 1990). This result suggests that the hairpins themselves or the initial helix formed between the nucleotides may be stabilized by Mg^{2+}, but also indicates that tertiary structures are probably not required. In contrast, tertiary structure may be required in the RNA I–RNA II pairing reaction from the plasmid Col E1. The pairing reaction is Mg^{2+}-dependent (Tomizawa, 1984); and the stability of the initial complex formed between isolated hairpins derived from RNA I and RNA II is affected by mutations in both loop and stem nucleotides, even while complementarity and base composition are conserved (Eguchi & Tomizawa, 1991; Gregorian & Crothers, 1995). In addition, NMR analysis of the initial complex suggests that the interacting regions are stacked on the hairpin stems (Marino et al., 1995). Therefore, the precise structure of the loops and the complex formed between them may affect the stability of the initial loop–loop complex and, thus, the pairing rate.

Our results suggest that Mg^{2+} stabilizes tertiary structure involving sar RNA loop II; the placement of the other Mg^{2+} cannot be assigned. The dissociation constant for the low-affinity site is about 30 mM. This value is similar to the value for Mg^{2+}-dependent tertiary structure involving sar RNA loop II; therefore, this loop is a good candidate for a structure required for pairing. The dissociation constant for the high-affinity site is about 2 mM; this dissociation constant could correspond to Mg^{2+} binding to sar RNA tertiary structure involving loop I or the interhairpin region, or to (as yet unidentified) ant RNA tertiary structure.

It is not known if Mg^{2+} is required to stabilize one or both of the initial complexes between the loops. Mg^{2+} is known to stabilize the complex between model hairpins derived from the Col E1 RNA I and RNA II (Gregorian & Crothers, 1995); thus, it is possible that Mg^{2+} is acting this way in the sar RNA–ant RNA pairing reaction. The two Mg^{2+} ions that are inferred from the Mg^{2+}-dependence of the pairing reaction are probably involved in stabilization of tertiary structure. However, it is possible that binding of additional Mg^{2+} ions is required for maximal pairing rates, and that these ions are required to stabilize initial complex(es). If so, the dissociation constant(s) for binding of Mg^{2+} ion(s) to these site(s) would have to be between 2 and 30 mM.

The in vivo mechanism of inhibition

Formation of the initial, reversible complex is probably not sufficient to exert antisense control. Sar RNA nt 13 and 14 pair to the Shine–Dalgarno ribosome binding sequence in the initial, reversible complex. Thus, it is possible that binding of sar RNA to ant RNA in the initial complex could compete with binding of the ribosome to ant RNA, and that the competition would be sufficient to establish antisense control. This possibility is supported by the observation that formation of the transient complex is sufficient for antisense control in the Col E1 RNA I–RNA II system (Lin-Chao & Cohen, 1991). However, it should be noted that antisense control in this case does not involve competition with a ribosome. The effect of the sar RNA loop I mutations on K_d suggests that formation of the reversible complex is not sufficient to exert control in the sar RNA–ant RNA control system. Both sar RNA loop I mutations have been shown to reduce the ability of sar RNA to reduce *ant/lacZ* gene expression in vivo (M.M. Susskind, pers. comm). Because these mutations also increase the strength of the initial, reversible interaction, it appears unlikely that formation of the transient complex is sufficient to exert antisense control.

Factors other than the rate of formation of the first stable complex or the fully paired duplex probably affect the ability of sar RNA to exert antisense control. The ratio of the mutant k_2/K_d value to the wild-type k_2/K_d value describes the relative rate of formation of the first stable complex with the mutant sar RNA in the limit of low ant RNA concentration. Although both the 12U → A (relative k_2/K_d = 0.92) and the 13C → U (relative k_2/K_d = 0.38) mutations cause reductions in the value of k_2/K_d, the magnitude of the effect is not as large as the effect observed in vivo: both the 12C → U mutation and the 13C → U mutation impair the ability of multicopy sar RNA to reduce *ant/lacZ* expression by about fivefold (M.M. Susskind, pers. comm.). In addition, the relative rate of formation of the fully paired duplex does not explain the observed in vivo defects, because the k_3 values observed in pairing reactions with wild-type and mutant RNAs are the same within error.

Several factors could explain the lack of correlation between the kinetic parameters measured in vitro and the level of control observed in vivo. First, it is possible that the mutations affect the sar RNA concentration achieved in vivo. Although this possibility has not been investigated extensively, mutant RNA concentrations in vivo are within twofold of wild-type RNA concentrations (M.M. Susskind, pers. comm.), suggesting that relative RNA levels are not the explanation for the lack of proportionality between the k_2/K_d value and the observed level of control. Second, it is possible that pairing may be affected by a protein factor like the Rom protein that increases the strength of the initial, transient interaction between the Col E1 RNA I and RNA II (Eguchi & Tomizawa, 1990; Tomizawa, 1990a). If this were the case, the kinetic values measured in our system would not reflect the actual in vivo pairing reaction. Third, it is possible that RNA folding and pairing take place simultaneously, and that the in vitro folded structures of sar RNA and ant RNA do not reflect the in vivo structures. Finally, binding of divalent cations may be altered in the mutant RNAs. If the binding of ions or other small cofactors were different in each mutant, the observed larger-than-predicted loss of control and lack of correlation between k_2/K_d levels and control might be explained.

MATERIALS AND METHODS

Reagents and enzymes

Tris-HCl, Tris base, KCl, $CoCl_2$, putrescein, spermidine, spermine, and cytidine 3′-monophosphate (Sigma), $MgCl_2$, $ZnCl_2$, $SrCl_2$, $CaCl_2$, glycerol, chloroform, and dimethylsulfoxide (Fisher), $MnCl_2$ (J.T. Baker Chemical Co.), EDTA (ICN Biochemicals), ATP (Pharmacia LKB Biotechnology), acrylamide (Bio-Rad), formamide and proteinase K (Boehringer-Mannheim), phenol (International Biotechnologies, Inc.), bromphenol blue and xylene cyanol (Schwartz-Mann Biotechnology), [γ-^{32}P]-ATP (Amersham), *Escherichia coli* total tRNA (Boehringer-Mannheim), T4 RNA ligase (United States Biochemical Co. or Bethesda Research Laboratories), SDS (Bio-Rad), and NaOH, KOH, and perchloric acid (Baker) were purchased from the sources indicated.

RNA synthesis, labeling, and purification

The DNA constructs used, RNA synthesis, 5′ end-labeling, and RNA purification were described in Schaefer and McClure (1996). RNAs were 3′ end-labeled with cytidine 3′, 5′-[5′-^{32}P] bisphosphate (pCp) and T4 RNA ligase. [5′-^{32}P] pCp was made from cytidine 3′-monophosphate (Cp) by incubating 160 μM Cp, 160 μM [γ-^{32}P]-ATP (typically 3 × 10^5 Cerenkov cpm/pmol), and 10 units polynucleotide kinase in 10 μL in the buffer supplied by the manufacturer (kinase buffer) at 37 °C for 30 min. The pCp was used in the ligation step without further purification. RNA ligation reactions contained 109 μM pCp, 1.1 μM sar RNA, 1.5 M dimethyl sulfoxide, 1.1 mM ATP, and 20 units RNA ligase in kinase buffer in 14 μL. Reactions were incubated at 37 °C for 2 h.

Measurement of pairing rate by the electrophoretic mobility shift (gel-shift) assay

Initiation of pairing reactions was done in two ways. In both cases, RNA pairing reactions contained the indicated amounts of ant RNA and ≤ 1.5 nM 5′ end-labeled sar RNA (typically >1,000 Cerenkov cpm/lane). The RNAs were pretreated by heating to 95 °C for 2 min, followed by quick chilling on ice. In the experiments of Figures 1, 4, and 6, the RNAs were incubated separately for 20 min in pairing buffer with Mg^{2+} (20 mM Tris-HCl, pH 8.0, 100 mM KCl, 8 μg/mL tRNA, and the indicated concentrations of $MgCl_2$). Pairing was initiated

by the addition of sar RNA to ant RNA. The samples taken for time = 0 in all experiments contained only sar RNA; pairing buffer was added to sar RNA in place of the ant RNA. In the experiments of Figures 8, 9, and Table 2, the RNAs were incubated in pairing buffer without Mg^{2+} (20 mM Tris-HCl, pH 8.0, 100 mM KCl, and 8 μg/mL tRNA) at 37 °C for 20 min. Pairing reactions were initiated by addition of sar RNA to ant RNA, followed by immediate addition of the indicated divalent cation or polyamine. Preincubation of the RNAs with Mg^{2+} and initiation of the reaction with Mg^{2+} yielded the same pairing rate (data not shown). For pairing reactions that contained a single polyamine or divalent cation (the experiments of Fig. 8 and Table 2), the ant and sar RNAs were together for only 0.15 min before the cation was added. The maximum rate constant k_{obs} in the absence of divalent cation was 0.22 min^{-1} (at 500 nM ant RNA; Schaefer, 1996); thus, less than 5% of the sar RNA in any experiment became paired in the 0.15 min required to add the polyamine or cation. For pairing reactions that contained both polyamine and Mg^{2+} (the experiments of Fig. 9), the RNAs were together for 0.5 min before addition of Mg^{2+}. Because k_{obs} at 15 nM ant RNA in the presence of the polyamines used was < 0.05 min^{-1} (Fig. 8), less than 2% of the sar RNA became paired before addition of the Mg^{2+}.

In all experiments, 10-μL portions of the reaction were removed at various times and the pairing reaction was terminated by the addition of 2 μL of stop solution (30% glycerol, 100 mM EDTA, 0.2% xylene cyanol, and 0.2% bromphenol blue) plus 1 μL 0.5 M EDTA. For reactions containing polyamines, the samples were also quick frozen in a dry ice/ethanol bath, followed by thawing just until the sample became liquid (the pairing reaction is strongly temperature dependent; Liao, 1988; Schaefer, 1996). In both cases, the reaction was immediately loaded on a 5% polyacrylamide (29:1 acrylamide:bis-acrylamide) slab gel (14 × 16 × 0.15 cm) and run at 150 V in TBE running buffer (0.09 M Tris-borate, pH 8.5, and 0.002 M EDTA). Gels were dried onto Whatman 3MM paper and quantitated using an AMBIS 4000 Radioanalytic Scanner (Scanalytics). For some experiments, an image was also made by exposing Kodak X-O-MAT film to the gel.

Measurement of pairing rate by the RNase protection assay

RNA pairing reactions were performed with ≥ 15 nM ant RNA and ≤ 1.5 nM 5′ or 3′ end-labeled sar RNA (wild-type, mutant, or a mixture of limited alkaline hydrolysis products). Typical experiments contained 5,000–10,000 Cerenkov cpm/lane. RNAs were pretreated by heating to 95 °C for 2 min, followed by quick chilling on ice. The RNAs were then incubated in pairing buffer (20 mM Tris-HCl, pH 8.0, 100 mM KCl, 10 mM $MgCl_2$, and 8 μg/mL tRNA) at 37 °C for 20 min. Pairing reactions were initiated by the addition of ant RNA to sar RNA. Zero-minute time points contained only sar RNA; pairing buffer was added to sar RNA in place of the ant RNA. At various times, portions of the reaction were removed and the pairing reaction was terminated by the addition of 40–124 μg/mL (ss-specific) RNase A. Under these conditions, sar RNA underwent > 5 cleavages/molecule within 7.5 s (data not shown); thus, the pairing reaction was quickly quenched by elimination of intact RNAs. After a ≥ 10-min incubation, the RNase digestion reactions were terminated by adding SDS to a final concentration of 0.55% and proteinase K to a final concentration of 0.14 mg/mL. The samples were then incubated at 37 °C for 20 min. Proteinase K was removed from the samples by extraction with an equal volume of phenol and chloroform (1:1); the RNA was then precipitated with ethanol. The pellet was dissolved in equal volumes of pairing buffer and loading buffer (80% formamide, 10 mM NaOH, 1 mM EDTA, 0.1% xylene cyanol, and 0.1% bromphenol blue), heated to 95 °C for 2 min, quickly chilled on ice, and run on a polyacrylamide/7 M urea sequencing (31 × 38.5 × 0.04 cm, 8–12.5% 19:1 acrylamide:bis-acrylamide) gel at 60 W in running buffer. A size ladder made by alkaline hydrolysis of sar RNA was loaded along with the digestion reactions.

Alkaline hydrolysis of RNA

Limited alkaline hydrolysis was performed at 95 °C for 2–3 min in 25 mM KOH. The hydrolysis reaction was then terminated by placing the reaction at 4 °C. The cleavage reaction was completed by adding perchloric acid ($HClO_4$) to a final concentration of 29 mM. Following a 15-min incubation at 4 °C, the reaction was neutralized with Tris base; the RNA was then precipitated with ethanol. If the RNA was to be used as a marker, the resultant RNA pellet was dissolved in equal volumes of pairing buffer and loading buffer and loaded on the gel. If the RNA was to be used in RNase protection experiments, the pellet was dissolved in a solution of 10 mM Tris-HCl, pH 8, and 0.1 mM EDTA.

Calculation of rate constants

Pseudo-first-order rate constants (k_{obs}) for the sar RNA–ant RNA pairing reaction were measured in two types of experiments. Rate constants for intact sar RNA–ant RNA pairing reactions were measured by gel-shift assay. Rate constants for pairing reactions with sar RNA length variants created by limited alkaline hydrolysis were measured with the RNase protection assay. For the gel-shift assay experiments, ln (fraction total lane cpm in the sar RNA band) was plotted versus time; for the RNase protection experiments, ln (cpm in band n/cpm in band n in the no RNase lane) was plotted versus time. In both cases, the slope = $-k_{obs}$.

Calculation of K_d and k_2 from gel-shift assay experiments

K_d and k_2 values were determined from plots of k_{obs} versus ant RNA concentration (Figs. 1 and 4, and the experiments of Table 2). For the following mechanism,

$$A + S \underset{k_{-1}}{\overset{k_1}{\rightleftharpoons}} C_t \xrightarrow{k_2} \text{stably paired complex(es)},$$

with ant RNA in excess,

$$k_{obs} = \frac{k_1 \cdot k_2 \cdot A_0}{k_{-1} + k_2 + k_1 \cdot A_0}, \quad (1)$$

(Strickland et al., 1975) where k_1, k_{-1}, and k_2 are rate constants for the individual steps and A_0 = the concentration of ant RNA in the reaction. Given that the dissociation constant (K_d) for the first reversible step is k_{-1}/k_1 and assuming that the initial step is in rapid equilibrium compared to the rate of the second step, ($k_{-1} \gg k_2$):

$$k_{obs} = \frac{k_2 \cdot A_0}{K_d + A_0} \quad . \tag{2}$$

K_d and k_2 were determined by fitting the data to an equation analogous to the Scatchard equation:

$$\frac{k_{obs}}{A_0} = \frac{k_2}{K_d} - \frac{k_{obs}}{K_d} \quad . \tag{3}$$

A plot of k_{obs}/A_0 versus k_{obs} was a straight line with slope = $-1/K_d$; k_2 = −intercept/slope. The slope and intercept were determined using the linear least-squares regression from the Kaleidagraph (Synergy Software) graphing program. Standard deviations in the slope and intercept of the line were propagated according to Bevington (1969). Because the value of k_2 determined in this way was very small (12 min^{-1}), we believe that the rapid equilibrium assumption was reasonable.

The value of k_{obs} reached a plateau at high concentrations of spermine (Fig. 8) and at high concentrations of Mg^{2+} in the presence of putrescein or spermidine (Fig. 9). Equations 2 and 3 were also used to analyze the experiments of Figures 8 and 9. In these cases, $k_2 = k_{obs}$ at saturating cation concentrations and K_d = the dissociation constant for the interaction between RNA and the cation. A small background value of k_{obs} (=0.01 min^{-1} in the absence of cation) was subtracted from all k_{obs} values before analysis.

Calculation of k_3 from RNase protection experiments

The value of k_3 was determined from RNase protection experiments (Figs. 2, 4), using the values for K_d and k_2 determined as described above. For the following mechanism,

$$A + S \overset{K_d}{\rightleftharpoons} C_t \xrightarrow{k_2} C_c \xrightarrow{k_3} AS \quad ,$$

with ant RNA in excess,

$$\frac{C_c}{S_0} = \frac{k_{obs}}{(k_3 - k_{obs})} e^{-k_{obs} \cdot t} + \frac{k_{obs}}{(k_{obs} - k_3)} e^{-k_3 \cdot t} \tag{4}$$

and

$$\frac{AS}{S_0} = \left\{ 1 + \frac{1}{(k_{obs} - k_3)} \cdot (k_3 \cdot e^{-k_{obs} \cdot t} - k_{obs} \cdot e^{-k_3 \cdot t}) \right\} \tag{5}$$

(Amdur & Hammes, 1966), where $k_{obs} = k_2 A_0/(K_d + A_0)$, t = time, K_d = the dissociation constant for the first reversible step, A_0 = the concentration of ant RNA in the reaction, and S_0 = the initial concentration of sar RNA in the reaction. Theoretical curves for the time course of appearance of AS and for the appearance and disappearance of the intermediate C_c were generated, using the above equations with the known values for K_d, k_2, and A_0, and various values for k_3. The value of k_3 was estimated by determining what value of k_3 resulted in AS and C_c curves that, when compared to the data, gave the minimum chi-square deviation. Final k_3 values reported are the result of multiple independent determinations; the error of the mean was calculated according to Bevington (1969).

Analysis of sigmoidal curves

The value of k_{obs} varied sigmoidally with Mg^{2+} concentration (Fig. 6). The concentration of Mg^{2+} at half-maximal k_{obs} ($Mg_{1/2}$) and the Hill coefficient (n = the apparent number of Mg^{2+} cations acting cooperatively in the reaction) were determined by fitting the observed rate constants as a function of [Mg^{2+}] to the Hill equation:

$$k_{obs} = \frac{k_{max} \cdot (Mg)^n}{(Mg_{1/2})^n + (Mg)^n} \quad , \tag{6}$$

where k_{max} = the k_{obs} at saturating [Mg^{2+}]; and Mg = the concentration of Mg^{2+}. Because the value of k_{max} varied as much as 50% between RNA preparations, k_{obs} was normalized to the k_{max} value obtained with a particular RNA batch. In addition, when comparisons were made between k_{obs} values obtained in the presence of various cations (Figs. 8, 9; Table 2), all experiments were performed with the same preparation of RNA. A small background value of k_{obs} (=0.01 min^{-1} at 0 mM Mg^{2+}) was subtracted from all k_{obs} values before analysis. Values of k_{max}, $Mg_{1/2}$, and n were determined by the Kaleidagraph graphing program, using only those points between 10% and 90% of k_{max}.

Determination of individual dissociation constants for Mg^{2+} from the values of $Mg_{1/2}$ and n

We analyzed the Mg^{2+}-dependence data using the Adair equation describing the binding of two ligands (the minimum for the value of n observed):

$$\frac{k}{k_{max}} = \frac{(Mg/K_1) + (Mg^2/K_1 \cdot K_2)}{1 + ((2 \cdot Mg)/K_1) + (Mg^2/K_1 \cdot K_2)} \quad , \tag{7}$$

where Mg = the concentration of Mg^{2+} and K_1 and K_2 are the dissociation constants describing the binding of Mg^{2+} to the lower- and higher-affinity binding sites, respectively. For this equation,

$$\log(Mg_{1/2}) = \frac{\log K_1 + \log K_2}{2} \quad \text{and} \quad ((2/n) - 1)^2 = K_2/K_1 \tag{8}$$

(Levitsky, 1978). Standard deviations of the $Mg_{1/2}$ and n values were propagated to determine a range for the K_1 and K_2 values.

ACKNOWLEDGMENTS

This work was supported by a grant from the National Institutes of Health (GM30375); K.L.S. was supported by a NIH predoctoral training grant (GM08067). We are grateful to Melissa Green for expert technical assistance.

Received August 6, 1996; returned for revision September 19, 1996; revised manuscript received November 12, 1996

REFERENCES

Amdur I, Hammes GG. 1966. *Chemical kinetics*. New York: McGraw-Hill Book Co.

Bevington PR. 1969. *Data reduction and error analysis for the physical sciences*. New York: McGraw-Hill Book Company

Cantor CR, Schimmel PR. 1980. *Biophysical chemistry part III: The behavior of biological macromolecules*. New York: W.H. Freeman and Co.

Eguchi Y, Tomizawa Ji. 1990. Complex formed by complementary RNA stem-loops and its stabilization by a protein: Function of the ColE1 Rom protein. *Cell 60*:199–209.

Eguchi Y, Tomizawa Ji. 1991. Complexes formed by complementary RNA stem-loops. *J Mol Biol 220*:831–842.

Freier SM, Kierzek R, Jaeger JA, Sugimoto N, Caruthers MH, Neilson T, Turner DH. 1986. Improved free-energy parameters for predictions of RNA duplex stability. *Proc Natl Acad Sci USA 83*:9373–9377.

Gregorian RS Jr, Crothers DM. 1995. Determinants of RNA hairpin loop-loop complex stability. *J Mol Biol 248*:968–984.

Grosjean H, Soll DG, Crothers DM. 1976. Studies of the complex between transfer RNAs with complementary anticodons. I. Origins of enhanced affinity between complementary triplets. *J Mol Biol 103*:499–519.

Hjalt TAH, Wagner EGH. 1995. Bulged-out nucleotides in an antisense RNA are required for rapid target RNA binding in vitro and inhibition in vivo. *Nucleic Acids Res 23*:580–587.

Jacques JP, Susskind MM. 1991. Use of electrophoretic mobility to determine the secondary structure of a small antisense RNA. *Nucleic Acids Res 19*:2971–2977.

Jaeger JA, Turner DH, Zuker M. 1989a. Improved predictions of secondary structures for RNA. *Proc Natl Acad Sci USA 86*:7706–7710.

Jaeger JA, Turner DH, Zuker M. 1989b. Predicting optimal and suboptimal secondary structure for RNA. *Methods Enzymol 183*:281–306.

Kittle JD, Simons RW, Lee J, Kleckner N. 1989. Insertion sequence IS10 anti-sense pairing initiates by an interaction between the 5′ end of the target RNA and a loop in the anti-sense RNA. *J Mol Biol 210*:561–572.

Levitsky A. 1978. *Quantitative aspects of allosteric mechanisms*. Berlin: Springer-Verlag.

Liang LG, Gluick TC, Draper DE. 1994. Stabilization of RNA structure by Mg ions: Specific and non-specific effects. *J Mol Biol 237*:577–587.

Liao SM. 1988. Regulation of gene expression in the immunity I region of bacteriophage P22 [thesis]. Pittsburgh, Pennsylvania: Carnegie Mellon University.

Liao SM, Wu Th, Chiang CH, Susskind MM, McClure WR. 1987. Control of gene expression in bacteriophage P22 by a small antisense RNA. I. Characterization in vitro of the P_{sar} promoter and the *sar* RNA transcript. *Genes & Dev 1*:197–203.

Lin-Chao S, Cohen SN. 1991. The rate of processing and degradation of antisense RNA I regulates the replication of ColE1-type plasmids in vivo. *Cell 65*:1233–1242.

Marino JP, Gregorian RS Jr, Csankovszki G, Crothers DM. 1995. Bent helix formation between RNA hairpins with complementary loops. *Science 268*:1448–1454.

Persson C, Wagner EGH, Nordstrom K. 1988. Control of replication of plasmid R1: Kinetics of in vitro interaction between the antisense RNA, Cop A, and its target, Cop T. *EMBO J 7*:3279–3288.

Persson C, Wagner EGH, Nordstrom K. 1990. Control of replication of plasmid R1: Structures and sequences of the antisense RNA, Cop A, required for its binding to the target RNA, Cop T. *EMBO J 9*:3767–3775.

Schaefer KL. 1996. Kinetic and structural analysis of a bacteriophage P22 antisense RNA pairing reaction [thesis]. Pittsburgh, Pennsylvania: Carnegie Mellon University.

Schaefer KL, McClure WR. 1997. Antisense RNA control of gene expression in bacteriophage P22. I. Structures of sar RNA and its target RNA, ant mRNA. *RNA 3*:141–156.

Siemering KR, Praszkier J, Pittard AJ. 1994. Mechanism of binding of the antisense and target RNAs involved in the regulation of IncB plasmid replication. *J Bacteriol 176*:2677–2688.

Strickland S, Palmer G, Massey V. 1975. Determination of dissociation constants and specific rate constants of enzyme–substrate (or protein–ligand) interactions from rapid reaction kinetic data. *J Biol Chem 250*:4048–4052.

Sugiyama T, Itoh T. 1993. Control of ColE2 DNA replication: In vitro binding of the antisense RNA to the Rep mRNA. *Nucleic Acids Res 21*:5972–5977.

Teeter MM, Quigley GJ, Rich A. 1981. The binding of metals to tRNA. In: Eichorn GL, Marzilli LG, eds. *Metal ions in genetic information transfer*. New York: Elsevier/North-Holland. pp 233–272.

Thisted T, Sorensen NS, Wagner EGH, Gerdes K. 1994. Mechanism of post-segregational killing: Sok antisense RNA interacts with Hok mRNA via its 5′-end single-stranded leader and competes with the 3′-end of Hok mRNA for binding to the *mok* translational initiation region. *EMBO J 13*:1960–1968.

Tomizawa Ji. 1984. Control of ColE1 plasmid replication: The process of binding of RNA I to the primer transcript. *Cell 38*:861–870.

Tomizawa Ji. 1990a. Control of ColE1 plasmid replication: Interaction of Rom protein with an unstable complex formed by RNA I and RNA II. *J Mol Biol 212*:695–708.

Tomizawa Ji. 1990b. Control of ColE1 plasmid replication: Intermediates in the binding of RNA I and RNA II. *J Mol Biol 212*:683–694.

van Biesen T, Soderbom F, Wagner EGH, Frost LS. 1993. Structural and functional analyses of the FinP antisense RNA regulatory system of the F conjugative plasmid. *Mol Microbiol 10*:35–43.

Wu Th, Liao SM, McClure WR, Susskind MM. 1987. Control of gene expression in bacteriophage P22 by a small antisense RNA. II. Characterization of mutants defective in repression. *Genes & Dev 1*:204–212.

Zuker M. 1989. On finding all suboptimal foldings of an RNA molecule. *Science 244*:48–52.

RNA (1997), 3:175–185. Cambridge University Press. Printed in the USA.

Nuclear pre-tRNA terminal structure and RNase P recognition

YOON LEE, DAVID W. KINDELBERGER, JAE-YONG LEE, SHANNA McCLENNEN, JOEL CHAMBERLAIN, and DAVID R. ENGELKE

Department of Biological Chemistry, The University of Michigan, Ann Arbor, Michigan 48109-0606, USA

ABSTRACT

Nuclear pre-tRNA transcripts often contain an extension of the aminoacyl stem formed by base pairing between the 5′-leader and 3′-trailing sequences, but the −1 position preceding the mature 5′ end is usually left unpaired. Considering recently proposed tertiary structural models for RNase P RNAs, we hypothesize that the −1 mismatch prevents a strong, coaxially extended aminoacyl stem, which might otherwise sterically interfere with substrate positioning in the RNase P active site. This hypothesis is tested by creating uninterrupted aminoacyl stem extensions in four nuclear tRNA precursors that normally have a mismatched nucleotide at position −1, and comparing their cleavage rates with those of the normal precursors. Determinations of K_m and k_{cat} values for a normal and an altered pre-tRNA^{SUP53}, which exhibits the most subtle structural alteration immediately upstream of the cleavage site, indicate that the mismatch at position −1 is an important structural requirement for both substrate affinity and efficient catalysis (and/or product release) by nuclear RNase P. This conclusion is further supported in vivo, where the pre-tRNA^{SUP53} mutant precursor lacking the −1 mismatch is shown to accumulate.

Keywords: enzyme–substrate interaction; kinetic constants; nuclear RNase P; pre-tRNA structure

INTRODUCTION

The 5′-leader sequences from precursor tRNA molecules are processed by RNase P, a ribonucleoprotein endonuclease (Altman, 1989). In eubacteria, the RNA moiety of RNase P alone is catalytically active (Guerrier-Takada et al., 1983), whereas eukaryotic and archaebacterial enzymes bind and cleave substrates only in the context of holoenzymes (Darr et al., 1992). RNase P is unique among known ribozymes in that it recognizes conserved tertiary structural features of its substrates, rather than utilizing base pairing complementarity, and so can accurately process a large number of different pre-tRNAs of unrelated sequence. A full understanding of enzyme–substrate interaction, therefore, can only be achieved after elucidating the higher-order structural requirements of both catalytic and substrate RNAs. Toward this goal, secondary structures of the general eubacterial RNase P RNA (James et al., 1988; Hass et al., 1994) and yeast nuclear RNase P RNAs (Tranguch & Engelke, 1993; Tranguch et al., 1994) have been established, and the three-dimensional working models of the *Escherichia coli* M1 RNA (Harris et al., 1994; Westhof & Altman, 1994) and *Saccharomyces cerevisiae* RNA (Pagán-Ramos et al., 1995) have been proposed recently.

Examination of numerous mutations in pre-tRNAs has defined substrate sequences and/or structural determinants critical for both binding and catalytic process. As predicted by Altman et al. (1975), mutations resulting in an impairment of folding capacity of the mature tRNA domain disrupt the substrate–enzyme interaction (Kirsebom & Altman, 1989). Studies have demonstrated the significance of a coaxial stem formed by the aminoacyl and T-stem for recognition by the M1 RNA, as well as important contact points in the T-loop of the precursor (McClain et al., 1987; Green & Vold, 1988; Kahle et al., 1990b; Thurlow et al., 1991; Holm & Krupp, 1992; Kirsebom & Svärd, 1992). Mutations in the aminoacyl stem have been shown to affect RNase P cleavage (Nichols et al., 1988; Carrara et al., 1989; Drainas et al., 1989; Krupp et al., 1991), and direct contact points between this coaxial stem and RNase P RNA have been explored (Kahle et al., 1990a, 1990b; Gaur & Krupp, 1993; Nolan et al., 1993; Harris et al., 1994; Hardt et al., 1995).

Past the coaxial stem, it is known that interactions between the eubacterial RNase P RNA and the 3′ CCA termini encoded in eubacterial pre-tRNA transcripts

Reprint requests to: David Engelke, Department of Biological Chemistry, The University of Michigan, Ann Arbor, Michigan 48109-0606, USA; e-mail: engelke@umich.edu.

affect substrate recognition (Kirsebom & Svärd, 1994; Svärd et al., 1996). This aspect of enzyme–substrate recognition is not pertinent to the eukaryotic nuclear RNAs, however, where the CCA is not normally encoded in the tRNA gene. Rather, we have noted that, in yeast nuclear pre-tRNAs, the 5′-leader sequences are rich in purines and exhibit high base pairing potential with the pyrimidine-rich 3′-trailer containing the U_5 Pol III terminator (Geiduschek & Tocchini-Valentini, 1988). Interestingly, precursors that can support strong coaxial extensions from the aminoacyl acceptor stem display a helical break immediately upstream of the cleavage site. In this study, we hypothesize that this helical break or the mismatch at position −1 is necessary for proper positioning of these tRNA precursors into the active site of nuclear RNase P and we show, both in vitro and in vivo, that it is indeed one of the important structural requirements for efficient substrate recognition by the enzyme.

RESULTS AND DISCUSSION

We have surveyed 52 yeast tRNA genes to look for consensus structure beyond the mature tRNA domain that may indicate some aspects of functional importance. The survey revealed that most pre-tRNAs had potential to form base paired structures between the predicted 5′-leader and 3′-trailing regions (Table 1). The actual existence of this pairing has been further suggested by the resistance of precursors to 3′ exonucleolytic trimming in vitro (Engelke et al., 1985) and in vivo (Lee et al., 1991) before the 5′-leader is removed by RNase P. Of 52 sequences examined, however, 39 of them are unpaired at the −1 position, immediately 5′ of the cleavage site. Invariably, precursors containing a strong coaxial extension beyond the cleavage site are mismatched at the −1 position (Table 1; examples of strong predicted secondary structures are shown in Fig. 1A).

The fact that the other 13 sequences have the potential for a base pair at the −1 position indicates that the −1 mismatch is not a universally conserved structure that is absolutely required for function. However, five of the pre-tRNAs interrupt structure with bulges beginning with a nucleotide just opposite of the −1 position in the 3′-trailing region (denoted No^c in Table 1), and six others extend aminoacyl stems only by a single pair that is immediately followed by mismatched or bulged structure prior to a stem formation (No^e in Table 1). Two remaining sequences show a maximum of three or four extended base pairs of aminoacyl stem, but the formation of helical structure further downstream is not supported (Table 1; M17330, J01373). These observations suggest that the −1 mismatch may become an important structural prerequisite only in the presence of a strong coaxial extension of aminoacyl acceptor stem, but may not be a necessary component if the base paired structure is not supported beyond the cleavage site. In spite of these exceptions, the observation that a possible formation of strong coaxial extension of aminoacyl stem is always accompanied by a mismatch at position −1 is consistent with structural predictions of the eubacterial and nuclear tertiary structural models for enzyme–substrate interactions. Not only is the bacterially encoded 3′ CCA unpaired to interact with the enzyme in the case of the eubacterial RNase P RNA (Kirsebom & Svärd, 1994), but both eubacterial and eukaryotic models show possible steric interference if there was a coaxial extension of the aminoacyl stem, especially with helix P15 in the RNase P RNA (Harris et al., 1994; Pagán-Ramos et al., 1995).

Here, we postulate that the helix flexibility induced by the mismatch at position −1 allows some pre-tRNAs with particularly strong coaxial extensions to be accommodated effectively into the enzyme's active site structure. To test this hypothesis, we investigated the kinetics of yeast nuclear RNase P as a function of structural alteration in the aminoacyl stems of four nuclear pre-tRNA substrates: pre-$tRNA^{SUP53}$ (SUP53 allele of pre-$tRNA^{Leu3}$), pre-$tRNA^{Arg}$, pre-$tRNA^{Gly}$, and pre-$tRNA^{Tyr}$ (Fig. 1A). In previous analyses of yeast nuclear RNase P-substrate interaction (Newman et al., 1983; Strobel & Abelson, 1986a, 1986b; Leontis et al., 1988), we and others used directed mutations in the yeast pre-$tRNA^{SUP53}$ to identify structural features elsewhere in the substrate crucial to recognition and cleavage by RNase P in vitro. Pre-$tRAN^{SUP53}$ is a particularly useful substrate with which to test the need for a −1 helix disruption. A single nucleotide insertion, ∇A73, placed opposite of a bulged −1 residue, creates a strong coaxial extension (also denoted as "aa stem ext.") with minimal sequence perturbation (none at the cleavage site; Fig. 1B). Furthermore, the RNA has been shown previously to fold strongly into a single isoform and the solution structure of the mature tRNA domain has been determined (Lee & Knapp, 1985). Hence, a single nucleotide insertion outside the mature domain is not likely to cause major global structural alteration other than stabilizing a terminal helix extension of eight base pairs past the mature aminoacyl terminus. This speculation is reflected in the fact that both the pre-$tRNA^{SUP53}$ and ∇A73 variant yield single folding isoforms with minimal difference in migration rates in a nondenaturing polyacrylamide gel (Fig. 2A; compare WT versus aa stem ext. in the pre-$tRNA^{SUP53}$ panel). Further structural analyses using RNase V1, RNase ONE, and Pb^{2+} confirm the persistence of intact mature tRNA domain in the presence of the mutation (data not shown).

Strong coaxial extensions of the aminoacyl stem in the other three substrates (Fig. 1A) were constructed similarly by simultaneous substitution of 1–2 nt and insertion of 1–3 nt in the 3′-trailing regions. Because it